MODIFICATION OF STEELMAKING SLAG BY ADDITIONS OF SALTS FROM ALUMINUM
PRODUCTION

by

David C. Walker

Submitted in partial fulfillment of the requirements
for the degree of Master of Applied Science

at

Dalhousie University
Halifax, Nova Scotia
June, 2010

Canada

DALHOUSIE UNIVERSITY

TABLE OF CONTENTS

LIST OF FIGURES

LIST OF TABLES

LIST OF ABBREVIATIONS AND SYMBOLS

mm	Millimeter
μm	Micrometer
cP	Centipoise
EAF	Electric Arc Furnace
XRD	X-Ray Diffraction
EPMA	Electron Probe Micro-Analysis
EDS	Energy Dispersive Spectroscopy
WDS	Wavelength Dispersive Spectroscopy
ICP-OES	Inductively-Coupled Plasma Optical Emission Spectroscopy

ACKNOWLEDGEMENTS

ABSTRACT

The most common slag fluidizer in steelmaking is fluorspar, a mineral primarily composed of CaF_2. Because of increasing consumption and decreasing availability of cheap fluorspar, steelmakers are seeking alternative means of achieving slag fluidity. One possible alternative to fluorspar is spent salt from secondary aluminum production. This salt is obtained from the used flux in remelting aluminum scrap and dross. This material is widely available and considered toxic (meaning that use in steelmaking helps to reduce environmental impacts from disposal). This project is an investigation of spent salt as a replacement for fluorspar in slag-fluidizing applications by viscosity measurements and weight loss measurements at high temperatures (to evaluate the amounts of gases are formed). In addition, characterization of raw materials and melted slags by XRD, chemical analysis, and EPMA have been undertaken. The spent salt addition has a positive effect on slag fluidity, and shows promise for use in slags.

1.0 INTRODUCTION

1.1 MODERN STEELMAKING

Steelmaking is the most frequently practiced metal production in the world, accounting for more than 1 billion tonnes of steel annually[1]. This is a consequence of the great importance of steel in a multitude of applications. The manufacture of such large quantities of steel requires large quantities of slag, a complex oxide used to refine and thermally protect the underlying metal phase in each of the processing stages of liquid steel. The composition of the slag is of prime importance, especially in modern "clean" steelmaking practices, which allow for fine chemical control of the steel during processing.

1.2 STEELMAKING PROCESSES

Two types of steelmaking exist: integrated steelmaking, wherein raw iron ore is reduced in a blast furnace to make iron, which can then be further processed into steel; and non-integrated steelmaking, which typically uses an electric arc furnace (EAF) to remelt scrap steel, the main source of material. Integrated steelmaking accounts for approximately two-thirds of the steel produced in the world, while non-integrated plants produce the remainder[1]. Each of these processes is normally supplemented by a secondary steelmaking (also known as ladle metallurgy) process which allows for finer adjustment of the steel chemistry and temperature in preparation for casting[2]. In all of these

processes, the liquid steel (or iron) is in contact with slag, making the composition and characteristics of slags subjects of great concern to steelmakers. Steelmaking processes have been extensively studied, and detailed descriptions of each process are available[2,3,4].

1.2.1 STEELMAKING SLAGS

Slags are ionic liquid oxides used to control the composition of the steel during each step of the steelmaking process. Because of the immiscibility of these oxides in the metallic melt and their solubility in the slag, a slag is a second phase that allows products of oxidation reactions to be removed from the liquid metal. Slags can be formed by the more reactive components of ores which are not reduced in the blast furnace, or by mixed oxides of reactive metallic elements to make a synthetic slag. They perform multiple roles: a phase for collection and dissolution of oxidized components of the melt; a way of preventing oxidation of the iron melt; a method of introducing any non-metallic reactants to the system; a mechanism for refining the steel melt; and a layer of thermal insulation to keep the liquid steel from cooling quickly[2,3,4].

Slags have a number of properties that are beneficial to steelmaking operations. The heat capacities of most oxide slag components are high, and the thermal conductivities low. This means that heat can be conserved in the liquid metal-slag mixture, which is important for maintaining fluidity and homogeneity. One ramification of this is that the melting temperatures of some commonly used slags are relatively close to steelmaking

temperatures (~1600°C), so temperature stability is an important property. The low density of most slags helps in separation from the metal, since slags form an immiscible oxide phase floating on top of the metal. In addition to dissolving oxide phases, slags also have capacity to absorb sulfides, halides, and carbides. This is especially useful for desulfurization of steels, since the slag is a good medium with which to absorb the liquid sulfides formed, thus removing them from the steel[2,3].

1.2.2 FLUORSPAR IN STEELMAKING SLAGS

Fluorspar, a mineral made up of CaF_2 (when pure), has great relevance to modern steelmaking. The use of fluorspar in slags is widespread for two important reasons: fluorspar increases fluidity and decreases the melting temperature of the slag without changing its basicity, and therefore its capacity for desulfurization and deoxidation; and it dissolves high-melting solid slag components rather quickly, making slag liquefaction during heating a less time-consuming process[2,3,4].

1.3 ALUMINUM SMELTING

Aluminum production is second only to steel production in terms of tonnage, with primary production capacity for over 25 million tonnes annually[5]. The Hall-Héroult process for aluminum smelting has been the most widespread method of primary production for more than a century. This process uses high-temperature electrolysis to reduce alumina ore in a molten synthetic cryolite (Na_3AlF_6) bath[4,6]. The use of carbon

electrodes and cell lining allows the very corrosive cryolite to be used without rapid degradation of the cell.

Secondary aluminum is also a major contributor to total production, since the energy saved by using metallic feed rather than alumina can be as much as 95%[5]. Aluminum recycling processes normally use a flux based on sodium chloride-potassium chloride mixtures to melt secondary aluminum without contamination from the atmosphere[7,8,9]. Rotary or reverberatory furnaces may be used for this process, which has two important products: coalesced metallic aluminum that may then be remelted with primary aluminum to be cast into new products; and a sodium/potassium chloride salt containing aluminum, magnesium, iron, and calcium oxides.

1.3.1 WASTE FROM ALUMINUM PRODUCTION

One of the problems facing the aluminum industry is the considerable amount of waste produced when an electrolysis cell has degraded (over the course of several years[6,10,11]) and must be replaced. Degradation occurs by penetration of the carbon lining by sodium and electrolyte[6,10]. Once the cell is deemed to be unusable, it is reclaimed into 3 major fractions of waste: the frozen bath; the carbon lining, along with the material that has penetrated it; and the refractory brick surrounding the carbon, which must be removed to insert a new lining[6,10,11]. Currently, the "spent potlining" wastes generated are not suitable for general landfilling because of toxicity concerns; therefore, it is desirable to find alternative uses for the wastes[11]. The content of the

wastes from this source varies, but typically contains carbon, aluminum, aluminum oxide, and sodium as a fluoride, aluminate, or cyanide[10,12].

The main waste product of secondary aluminum reprocessing is a "spent salt", which contains sodium and potassium chloride, aluminum oxide, metallic aluminum, and small amounts of magnesium, calcium, iron, and silicon oxides[7,8,9]. There is also a small amount of fluoride content in this salt, as some fluorspar or cryolite is often added to aid in the consolidation of liquid aluminum and dissolution of aluminum oxide. This product is considered to be a toxic waste because of the solubility in water of some of the phases, and is therefore not landfilled[7,8,9].

Some preliminary testing and characterization of spent potlining as a steelmaking slag fluidizer has been done[12,13,14], and in one instance, measurements of viscosity of spent potlining without slag were done[15], but quantitative measurements of the viscosity of potlining-containing slag have not been reported in the literature. Similarly, characterization of the spent salt has been done, but no investigation of its potential effects in steelmaking slags has yet been undertaken.

1.4 THESIS OBJECTIVE

The objective of this thesis is to investigate the possibility of using spent salt from secondary aluminum production, as well as some other salts, for replacing fluorspar in fluidizing applications of steelmaking slags. It is hoped that, by using widely available

waste products such as spent salt or spent potlining, the consumption of fluorspar will be reduced to a more economical level. Also, the effects of reducing waste from the aluminum industry will have positive environmental effects. To this end, experiments have been done to determine whether some alkali salts are effective in fluidizing slags at high temperature. The salts used in the experiments were those commonly used in primary aluminum production (sodium/potassium aluminum fluoride) or secondary aluminum production (sodium/potassium chlorides and spent salt).

In addition, tests were done to evaluate the volatility of these salts, as the temperatures involved are much higher than those involved in aluminum processing, and gas formation would have important ramifications for safety and equipment degradation. Finally, evaluation of the compositions and phases of the slags before and after melting was done to compare the chemical and structural changes that took place in the liquid and during solidification.

2.0 THEORY

2.1 SLAG STRUCTURE AND BASICITY

Slags containing multiple cations show more complex behaviour than liquid oxides containing only one cation, since some cations have different relationships with oxygen than others. Those cations with higher valencies (such as Si^{4+}) tend to form extensive networks containing bridging oxygens (as SiO_4^{4-} complex anions, for example)[3,16,17]. The silicate network can be considered to be a polymer with each SiO_4^{4-} ion (known as the orthosilicate) constituting a monomeric unit. Increasing polymerization of these units increases the size and atomic weight of the network, and increases the negative charge of the network[3,17,18]. For example, $Si_2O_7^{6-}$ complex ions (or pyrosilicates) in a slag are made up of two SiO_4^{4-} ions that have been joined together by a bridging oxygen atom. These two kinds of ions are shown in Figure 2.1.

Orthosilicate   Pyrosilicate

● Si   ○ O
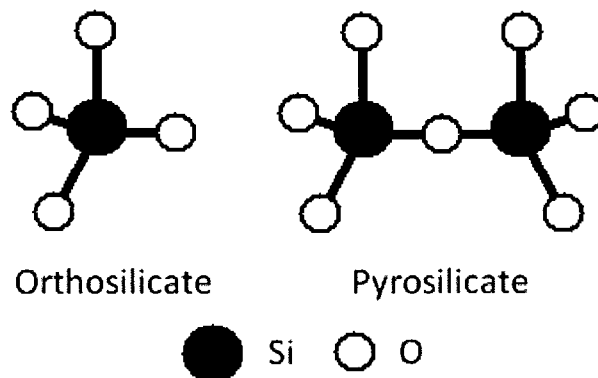
Figure 2.1 Relationship between orthosilicate (SiO_4^{4-}) and pyrosilicate ($Si_2O_7^{6-}$) ions.

As the polymerization of the silicate ions increases further, the ratio of bridging to non-bridging oxygen atoms increases, leading to silicates in chain, sheet, and finally three-dimensional networks. The larger molecular size of these complex ions makes mobility in the liquid difficult, while the net charge of the network also increases as more SiO_4^{4-} units are added. The total effect of the larger silicate unit and larger electrostatic charge (which again inhibits movement) is to decrease the fluidity of the liquid. A slag with high SiO_2 content is typified by this viscous behaviour, and is called acidic[17,18].

The behaviour of silica in isolation has been described, but the roles of other ions have not. Cations of metals with lower valencies and high oxygen affinities (like Ca^{2+} or Na^+) break the networks formed in slags by "donating" their oxide ions[18,19]. This depolymerization is shown in Figure 2.2. Because of the smaller silicate units formed in a slag with high CaO (or other similar oxide) content, the fluidity of these slags is increased greatly. A slag (and oxide) of this type is known as basic. Figure 2.3 compares schematic depictions of the structures of a basic slag and an acidic slag.
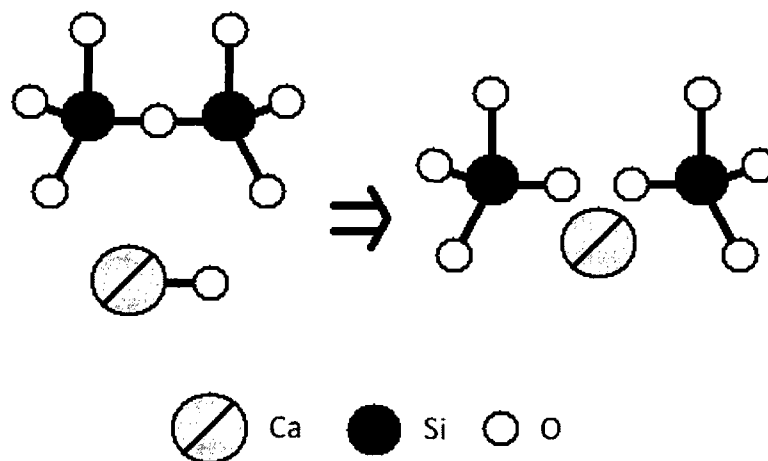
Figure 2.2 Depolymerization of pyrosilicate by addition of CaO.
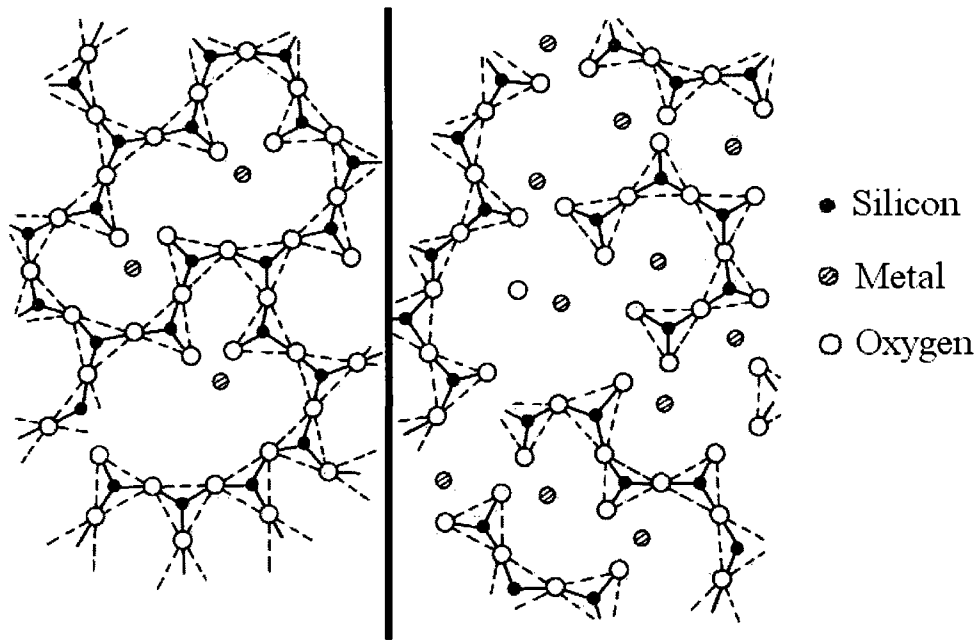
Figure 2.3 Structure of acidic slag (left) and basic slag (right), showing the varying degrees of networking possible in silicate slags[17].

Non-oxide slag components, most commonly fluorides, are also seen in steelmaking. The structural effects of these components are less well understood than those of mixed oxides. The effect of calcium fluoride is greater than that of calcium oxide in breaking the network of silicates, which is thought to be because the fluorine replaces non-bridging oxygen atoms and allows the replaced oxygen to further depolymerise the network. Some silicofluoride phases are volatile (as compared to the rest of the slag), and there is concern with the amount of volatile fluoride produced[3].

2.1.1 BASICITY

Basicity of a slag is a measure of the relative amounts of basic and acidic components in the slag. Several ways of measuring basicity exist, and many of these are empirically determined in practice[3]. A common method of expressing the basicity of a slag is the B-ratio, which is the ratio of weights of basic components to acidic components. A version of this ratio (most applicable for basic slags, where alumina behaves as an acidic component) is shown in (1)[3,4].

$$B = \frac{CaO + MgO}{SiO_2 + Al_2O_3} \tag{1}$$

In addition to determining the structure of the slag, the chemical composition of the slag influences reactions between the slag and metal. The usual reactions of concern in steelmaking processes are desulphurization and deoxidation[2,3]. In a basic slag (with high CaO activity), the desulphurization reaction shown in (2) is more favourable than in an acidic slag.

$$CaO\ (slag) + \underline{S} \rightarrow CaS\ (slag) + \underline{O} \tag{2}$$
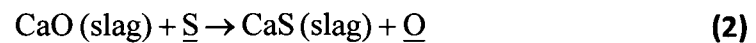
Likewise, the combined desulphurization and deoxidation of the steel, shown in (3), is also more favourable in a basic slag.

$$3CaO\ (slag) + 2\underline{Al} + 3\underline{S} \rightarrow 3CaS\ (slag) + Al_2O_3\ (slag) \tag{3}$$
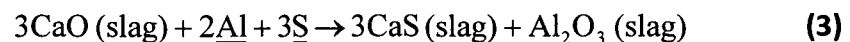
One of the main drawbacks of using a slag with high basicity is that the oxides which form basic slags, such as CaO and MgO, have melting points in excess of 2500°C[20,21]. Because of this, other oxides (normally silica) must be added to reduce the slag's

liquidus temperature to a more appropriate temperature for steelmaking. Since this also reduces the basicity of the slag, it is desirable for steelmakers to have a basic slag that is still entirely (or almost entirely) liquid at steelmaking temperature. Fluorspar, having a melting point of 1418°C[20], helps to lower the liquidus of the slag to a useful level without negatively affecting its basicity or fluidity[19,22,23].

The basicity and acidity of many oxides have been evaluated, both theoretically (according to their valence and electronegativity) and experimentally. Some basic oxides aside from CaO and MgO are Na_2O, K_2O, FeO, and MnO; acidic oxides other than the ubiquitous SiO_2 include P_2O_5, B_2O_3, and TiO_2[3,4].

2.2 VISCOMETRY OF SLAGS

Measurement of the rheological properties of liquids is crucial for many industries, since a fluid's characteristics can determine the success or failure of a process. Among the most important measurements used is viscosity, which defines the motion of a fluid in relation to applied stresses. In the case of steelmaking, the viscosity of a slag is a factor in achieving adequate separation between the slag and metal phases. Also, and more importantly, the rates of slag-metal reactions can be limited by convective mass transfer, meaning that the slag must be sufficiently fluid for significant convection to occur and for these reactions to happen in a reasonable amount of time[2,3,4,17].

2.2.1 ROTATIONAL VISCOMETRY

Viscosity is defined as the ratio of shear stress to shear rate, and can be measured by a variety of methods[25]. The rotational viscometer, in addition to being robust and simple in design, allows for continuous measurement (meaning that measurements can be made while other variables, such as temperature, are changed). The factors governing the behaviour of a Newtonian fluid in a concentric cylinder rotational viscometer are shown in (4).[25,26]:

$$\eta = \frac{Mx^2(R_C^2 - R_b^2)}{4\pi\omega R_b^4 R_c^2 L} \tag{4}$$

where η is the dynamic viscosity, M is torque (measured by the viscometer), x is the radius at which shear rate is calculated, R_c is the radius of the container, R_b is the radius of the spindle, ω is the angular velocity of the spindle, and L is the effective length of the spindle. L is a scaling factor based on the end effects of the spindle, since the rest of (4) assumes that the spindle and container are infinite tubes.

The rotational viscometer is most suited to evaluating Newtonian fluids[25,26]. However, the ability to use other rheological instruments (which might be better suited to measuring non-Newtonian fluids) at high temperature is rather limited by the possible materials of construction. This factor, combined with the simplicity and versatility of the rotational viscometer system, has led to the widespread use of this type of viscometer even in measurements of systems which are non-Newtonian, such as slags[16,19,22,23,27,28,29].

2.2.2 EFFECTS OF TEMPERATURE AND BASICITY ON VISCOSITY OF SLAGS

The effect of temperature on viscosity has been shown to follow an Arrhenius-type relationship for many fluids[17,25], which takes the form of (5):

$$\eta = Ae^{\frac{-Q}{RT}}$$

(5)

where η is the dynamic viscosity, A is a constant preexponential factor, Q is the activation energy, R is the ideal gas constant, and T is the temperature of the fluid. The negative exponent ensures that the viscosity decreases with increasing temperature, which is due to the increasing mobility of molecules in the fluid. This relationship is seen in slags of various compositions, including steelmaking slags with and without fluorspar as a fluidizer[16,19,22,23,24,27,28,29].

Slags containing large amounts of basic oxides (CaO or MgO) or large amounts of Al_2O_3 may not be entirely composed of liquid. The solids formed are often spinels ($MgAl_2O_4$) or alumina-rich, and can present problems with inclusions in casting or clogging of nozzles. In addition, the slag viscosity is heavily influenced by the solids content. The viscosity of slags (or other fluids) containing solids may be predicted using the Einstein-Roscoe equation, shown in (6)[25,30].

$$\eta = \eta_0(1 - af)^{-n}$$

(6)

where η is the viscosity of the solid-containing melt, η_0 is the viscosity of the solid-free melt, f is the volume fraction of solids, and a and n are experimentally determined constants. Values of n as high as 3.4[30] lead to strong dependence of the viscosity on solids content of the melt.

2.3 VOLATILITY OF SLAG COMPONENTS

Many constituents of slags are relatively stable in liquid form at steelmaking temperatures, due to their very low vapour pressures. However, there are some notable exceptions to this. One example of this is SiF_4, which has been identified as a major contributor to gas formation in fluoride-containing slags[3,31,32]. In slags containing alkali metals (especially potassium), problems arise in reducing conditions, when the alkali metals are reduced to a metallic vapour, which are then free to condense on any cooler surfaces[3,4]. As well, sodium and potassium halides tend to be more volatile than the corresponding calcium halides[20], so that addition of these alkali salts in a steelmaking furnace should lead to comparatively more vapour formation.

3.0 METHODOLOGY AND EXPERIMENTAL PROCEDURES

3.1 METHODOLOGY

The slags shown in Table 3-1, which were based on a master slag of CaO, MgO, and SiO_2, were prepared in order to do the experiments shown in Table 3-2. The slags used were fluidized by one of five substances: calcium fluoride (CaF_2), sodium aluminum fluoride (Na_3AlF_6), potassium aluminum fluoride ($KAlF_4$), spent salt from secondary aluminum production that was hand-cobbed to remove visible aluminum, and a synthetic spent salt of the same chemical composition as the spent salt used. The amount of fluidizer used (20%) was chosen for comparison with prior work and on appropriate slag melting temperatures for the viscometry tests. The tests to be done comprised high-temperature viscometry of each slag, weight loss measurements of the slags at high temperature and corresponding thermodynamic calculations, chemical analysis of raw materials and melted slags, and electron probe micro-analysis (EPMA).

Table 3-1 Slag compositions (by weight). CMS=CaO+MgO+SiO_2, F=CaF_2, N=Na_3AlF_6, K=$KAlF_4$, HC=hand-cobbed spent salt, SY=synthetic spent salt.

Slag component	CMS-F (%)	CMS-N (%)	CMS-K (%)	CMS-HC (%)	CMS-SY (%)
CaO	40	40	40	40	40
MgO	10	10	10	10	10
SiO_2	30	30	30	30	30
CaF_2	20	0	0	0	0
Na_3AlF_6	0	20	0	0	0
$KAlF_4$	0	0	20	0	0
Hand-cobbed spent salt	0	0	0	20	0
Synthetic spent salt	0	0	0	0	20

Table 3-2 Testing methodology. CMS=CaO+MgO+SiO$_2$, F=CaF$_2$, N=Na$_3$AlF$_6$, K=KAlF$_4$, HC=hand-cobbed spent salt, SY=synthetic spent salt.

Test	CMS Master Slag	Fluidizers	CMS-F	CMS-N	CMS-K	CMS-HC	CMS-SY
Viscometry	N	N	Y	Y	Y	Y	N
Weight loss and thermodynamic calculations	N	N	Y	Y	Y	N	Y
Chemical analysis	Y	Y	Y	Y	Y	N	Y
EPMA	N	N	Y	Y	Y	Y	N

3.2 MATERIALS AND SAMPLE PREPARATION

The materials used for the experiments belonged to one of two categories: master slag components and fluidizers. The master slag components were CaO (from MCB Reagents), SiO$_2$ (from Anachemia Chemicals), and MgO (from Alfa Aesar). The CaO was supplied as lumps of approximately 1 cm, while the SiO$_2$ and MgO were obtained as powders (<1mm in particle size). The fluidizers were CaF$_2$ (from Fisher Scientific), Na$_3$AlF$_6$ (from Alfa Aesar), KAlF$_4$ (supplied by Steel Dynamics Inc.), and spent salt from dross and recycled aluminum processing (supplied by Steel Dynamics Inc.). The spent salt was used in the hand-cobbed state (with the visible metallic aluminum picked out by hand). Finally, a synthetic spent salt was made by fusing a mixture of NaCl, KCl, Al$_2$O$_3$, CaF$_2$, MgO, and SiO$_2$, in proportions according to Table 3-3. This was done in order to prevent any contact between metallic aluminum from the spent salt and the platinum crucible used for weight loss experiments. The composition chosen was based on chemical analyses of the spent salt material as described in section 3.5.

Table 3-3 Synthetic spent salt composition (by weight), based on chemical analysis shown in Table 4-2.

	NaCl	KCl	Al_2O_3	MgO	SiO_2	CaF_2	Fe_2O_3
Composition (%)	22.9	13.7	47.4	4.8	6.5	2.8	1.9

3.2.1 SLAG PREPARATION

The moisture content of each master slag component (CaO, MgO, and SiO_2) was found by calcining 50 g of the oxide in a nickel crucible at 750 °C for 1 hour. The weights before and after calcining, measured with a Mettler BB2440 balance, for each master slag component, are shown in Table 3-4. Components for the master slag were subsequently weighed based on this weight change, meaning that if 100 g of CaO were desired in the slag, 110.29 g of CaO (prior to calcining) was required to be added. Once the master slag was prepared, the fluidizers were added to make the compositions shown in Table 3-1.

Table 3-4 Weight change after calcining of master slag components.

Slag component	Weight before calcining (g)	Weight after calcining (g)	Weight change (%)
CaO	50.00	45.34	9.33
MgO	50.00	45.81	8.38
SiO_2	50.00	49.90	0.21

After the proper weights were added, the mixture was placed into a steel shatterbox for 2 minutes to break up agglomerates and begin mixing of the components. The mixtures were then tumbled using a Turbula™ T2C shaker-mixer (shown in Figure 3.1) for 30 minutes to fully blend the powders. Finally, the blended powders were isostatically

compacted at 175 MPa in a Loomis cold isostatic press to increase interparticle contact and increase the green density (for better crucible loading).
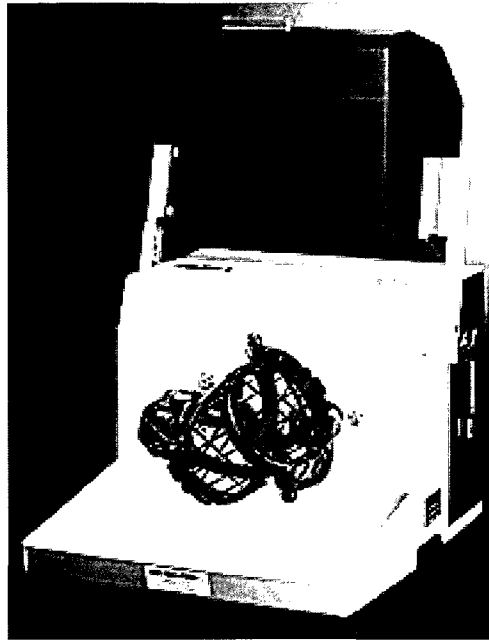
Figure 3.1 Turbula™ shaker-mixer.

3.3 VISCOMETRY

High-temperature viscosity testing was undertaken for each slag mixture, in order to determine whether the rheological characteristics of the slags were improved or worsened by the fluidizers chosen. In addition, samples obtained after viscosity testing could be used for microscopy.

3.3.1 APPARATUS

There were two major components to the apparatus used to test viscosity: the furnace and the viscometer (both shown in Figure 3.2). The furnace used was a Lucifer MeltMaster elevator furnace equipped with a Eurotherm programmable controller and type R (Pt/Pt-13%Rh) thermocouple. The viscometer was a Brookfield DV-II digital rotational viscometer, with a Strawberry-Tree data acquisition system which simultaneously recorded viscosity and temperature measurements.

Figure 3.2 Furnace (bottom) and viscometer (top right) used for slag viscosity experiments.
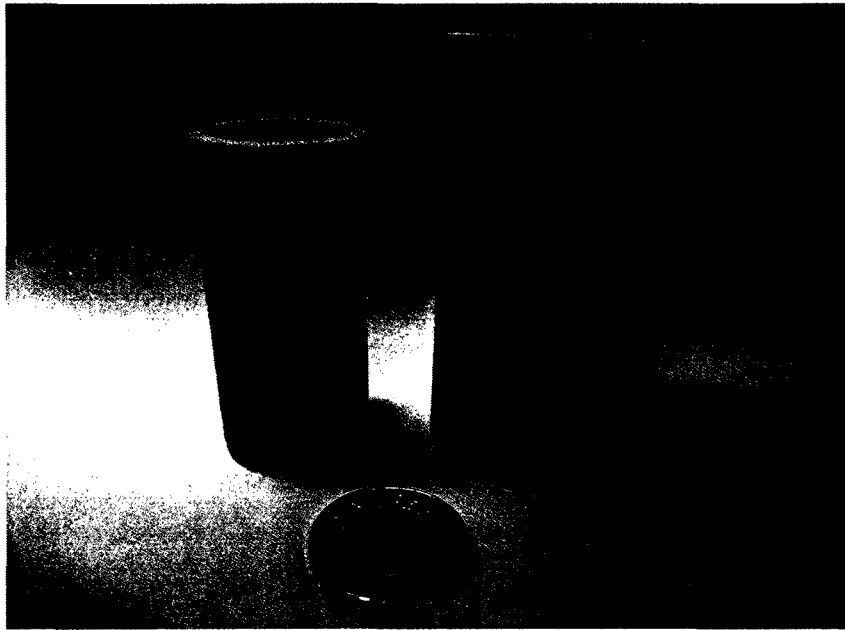
Figure 3.3 MgO crucible (left) and Al₂O₃ safety crucible (right).

MgO crucibles, with an inner diameter of 25 mm and height of 64 mm, were used to contain the slag at high temperature, and an Al_2O_3 safety crucible was used to ensure slag containment in case of breakage or spillage. Each of these crucibles is shown in Figure 3.3. The spindle was prepared from an alumina shaft with an inner diameter of 6.3 mm, an alumina tube with an outer diameter of 6.3 mm and a length of approximately 120 mm, and an iron hook. The alumina tube and shaft were joined using a paste of water and Sauereisen Adhesive Cement P-1, allowed to dry, then fired at 1450°C to secure the tubes. The iron hook was attached to the top of the spindle with platinum wire. The tubes used to assemble the spindle and an assembled spindle are shown in Figure 3.4, and a schematic of the arrangement of the furnace, viscometer, spindle, and crucibles is illustrated in Figure 3.5.
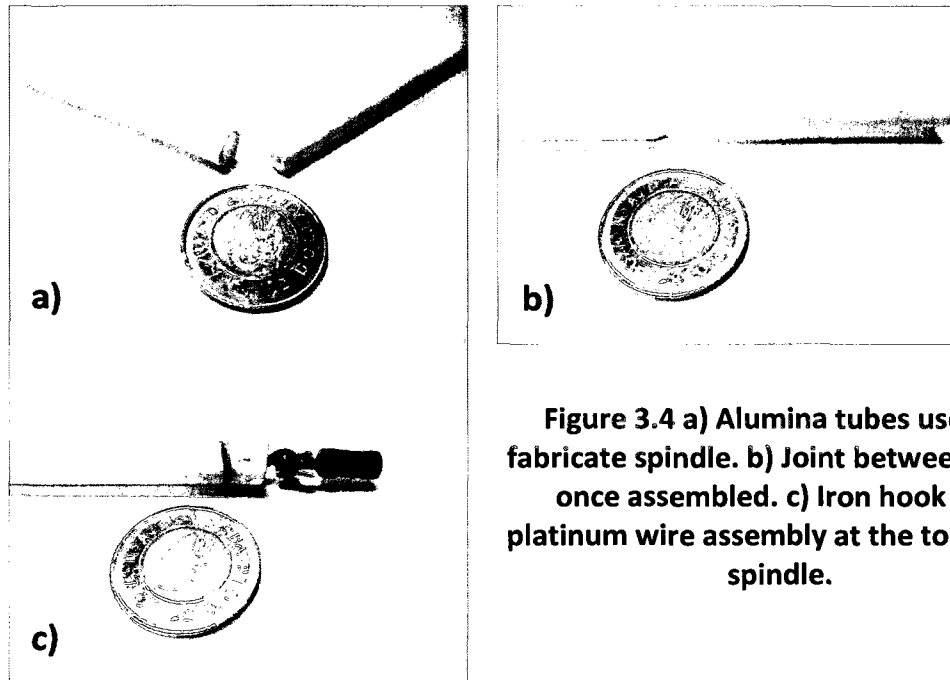
Figure 3.4 a) Alumina tubes used to fabricate spindle. b) Joint between tubes once assembled. c) Iron hook and platinum wire assembly at the top of the spindle.
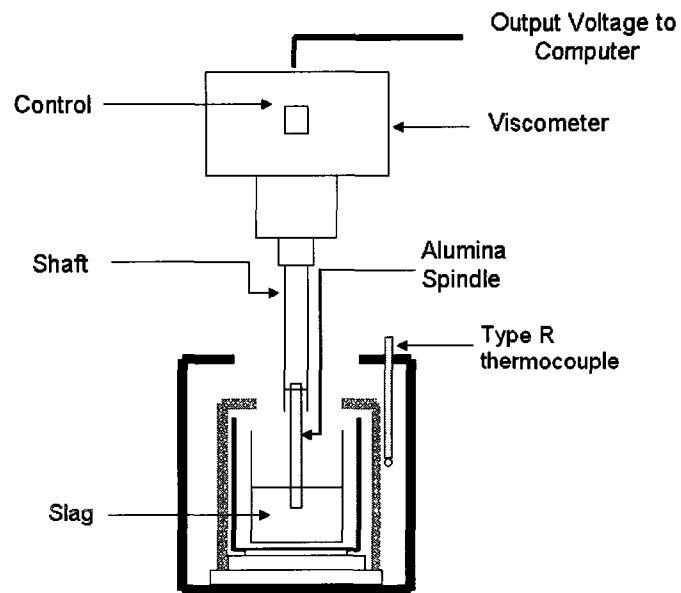
Figure 3.5 Schematic of furnace used for viscosity measurements.

3.3.2 TEST METHOD

Viscosity testing was done using a sample of approximately 40 g of compacted slag pellets, which corresponded to a depth of approximately 25 mm of melted slag in the crucible. The slag-containing crucible, safety crucible, and spindle were placed inside the furnace, and the furnace was heated to 1580 °C in 60 minutes. This temperature was held for 10 minutes, after which the spindle was lowered into the slag so that the end was approximately 12 mm from the bottom of the crucible. The viscometer was turned on at a rate of 30 rpm, data acquisition was started, and the temperature was reduced in a controlled manner to 1000 °C in 60 minutes. Once the viscosity increased beyond the range of the viscometer, the viscometer was turned off and data acquisition was stopped. The furnace was then cooled to room temperature and the crucible, spindle, and slag sample visually examined.

3.4 WEIGHT LOSS TESTING

Measurements of the weight loss of slags at high temperature were intended to relate the amount of volatile phase to the composition of the slag tested. These tests were meant to simulate heating of slag in an industrial environment, where large amounts of gas produced could be potentially hazardous to health and equipment. The melted slag samples obtained by this experiment were subsequently used for chemical analysis.

3.4.1 EQUIPMENT

The slag was heated in a 30 mL platinum crucible in a Deltech DT-31-RS-OS-E2404 furnace with $MoSi_2$ elements, Eurotherm 2404 programmable controller, and type R (Pt/Pt-13%Rh) thermocouple. The crucible and furnace are both shown in Figure 3.6. The weight before and after heating was measured on a Mettler BB2440 balance covered in fibrous insulation.

Figure 3.6 a) Platinum crucible used for weight loss experiments. b) Furnace used for weight loss experiments.

3.4.2 TEST METHOD

20 g of slag pellets were loaded into the platinum crucible and weighed. The temperature was raised to 600 °C and held for 30 minutes. After the holding period, the weight of the crucible and slag was measured again, and the crucible placed back into the furnace. This process was repeated with the same sample at intervals of 100 °C up to 1600 °C. Once the weight at 1600 °C was recorded, the slag sample was cooled,

removed from the crucible, and used for chemical analysis by XRD and ICP-OES. The crucible was immersed in HCl for 24 hours after each test to ensure that no contamination occurred from previous tests.

3.5 CHEMICAL ANALYSIS

Four techniques were used to determine the chemical compositions of the materials used: fluoride analysis using an ion selective electrode, chloride analysis using potentiometric titration, metallic element analysis by inductively-coupled plasma optical emission spectroscopy (ICP-OES), and phase determination using X-ray diffraction (XRD). The master slag was tested after blending, the other fluidizers were tested individually, and the chemistry of the melted slags from the weight loss measurements was tested after quenching and grinding to a particle size of <1mm.

3.5.1 FLUORIDE AND CHLORIDE ANALYSIS

The samples for fluoride analysis were fused in a mixture of Na_2CO_3 and KNO_3. The resulting products were then dissolved in nitric acid. The samples used for chloride analysis were fused in sodium peroxide, then dissolved in nitric acid. In the case of fluoride analysis, the solution was tested using a fluoride ion specific electrode; in the case of chloride analysis, potentiometric titration with silver nitrate was used.

3.5.2 ICP-OES

Chemical analysis of the samples for metal content was done using a Vista-Pro Varian ICP-OES system using an argon-based plasma and equipped with an SPS3 sample loading tray. The samples for analysis were either fused in sodium tetraborate and dissolved in nitric acid or subjected to a total acid (HCl, HF, HNO_3, and $HClO_4$) leach. The solutions were diluted to yield appropriate concentrations for the equipment prior to testing.

3.5.3 XRD

The phases present in the raw materials and the melted slags were analyzed using a Bruker D8 Advance XRD system. The materials to be tested were first ground to <1mm powder in a steel shatterbox. The powdered samples were then loaded into ridged sample holders. The tests were run at a scan rate of 0.1° per second using an accelerating voltage and beam current of 40 kV and 40 mA, respectively, with a copper X-ray source.

3.6 EPMA

EPMA was performed on selected samples that had been used for viscometry. The crucibles, which contained frozen-in slag samples and spindles, were sectioned into quarters using a diamond saw. The section used for microscopy included part of the crucible and spindle, so that any corrosion of the refractory materials could be

examined. The sectioned piece was then mounted in epoxy, polished with diamond suspensions, and subsequently carbon-coated.

EPMA was performed with a JEOL 8200 Superprobe electron probe instrument (shown in Figure 3.7) with both wavelength and energy dispersive spectrometers (WDS and EDS, respectively). The instrument was calibrated to detect Al, Ca, Cl, F, K, Mg, Na, O, and Si using mineral standards. Backscattered electron images were obtained and chemical analyses of individual grains were done for each of the samples. This technique also allowed for investigation of crucible and spindle corrosion in the slag.

Figure 3.7 EPMA instrument, showing sample chamber, spectrometers, and control and analysis systems.

4.0 RESULTS AND DISCUSSION

Results are divided into four groups: chemical analysis, viscometry results, weight loss measurements, and EPMA. Each of these is examined separately, then these results are synthesized into an analysis of the relationship between the viscosity, composition, and structure of each slag.

4.1 CHEMICAL ANALYSIS

4.1.1 FLUORIDE ANALYSIS, CHLORIDE ANALYSIS, AND ICP-OES

The results of fluoride and chloride analysis and the metals analysis for the slag fluidizers are shown in Table 4-1 and Table 4-2, respectively.

Table 4-1 Measured fluoride and chloride contents of each of the slag fluidizers used.

	CaF_2(%)	Na_3AlF_6(%)	$KAlF_4$(%)	Spent salt(%)
Fluoride content	9.26	3.68	34.40	1.43
Chloride content	<0.1%	<0.1%	<0.1%	4.5

The fluorine content of the CaF_2, Na_3AlF_6, and $KAlF_4$ fluidizers were significantly lower than would be expected by calculation according to atomic masses (which for these materials would be 48.7%, 54.3%, and 53.5%). Based on the analysis of the metal content of the fluidizers (shown in Table 4-2) and XRD results (detailed later in section 4.1.2), these fluidizers can be concluded to be solely CaF_2, Na_3AlF_6, and $KAlF_4$.

27

The fluoride content of the spent salt cannot be verified with such simplicity, since several metals were present and no fluoride phases were detected with XRD. Based on this and the knowledge that spent salt typically contains a few percent of a fluoride phase [7,8,9], the fluoride analysis was taken to be accurate for this component. This fluoride was analyzed to be 2.7% as calcium fluoride in Table 4-2, since calcium would form the most stable fluoride of any of the metals present, and is present in approximately the stoichiometric amount (which would be 2.93%, analyzed as CaF_2).

By calculating that the sodium and potassium present in the spent salt were both present as chlorides, the chloride percentage should be 14.7%, rather than 4.5%. However, if similar underestimation of the chloride content occurs as it does in the measurements of fluorine, then the actual chloride content may be this high (as would be expected from the use of a NaCl-KCl salt flux containing some alumina).

Table 4-2 Chemical analysis of metals in each of the slag fluidizers. Metal contents were calculated as either fluoride, chlorides, or oxides, as noted.

	CaF_2	Na_3AlF_6	$KAlF_4$	Spent salt
Al_2O_3/AlF_3	<0.1%	44.0% AlF_3	52.1% AlF_3	46.4% Al_2O_3
CaF_2	95.1% CaF_2	1.2% CaF_2	0.3% CaF_2	2.7% CaF_2
Fe_2O_3	<0.1%	<0.1%	<0.1%	1.9%
KF/KCl	<0.1%	0.1% KF	40.9% KF	13.4% KCl
MgO	<0.1%	0.21%	<0.1%	4.7%
NaF/NaCl	<0.1%	51.6% NaF	<0.1%	22.4% NaCl
SiO_2	<0.1%	0.89%	<0.1%	6.4%
Total	95.1%	98.0%	93.3%	97.9%

The fluoride and chloride contents and metals analysis of the melted slags are shown in Table 4-3 and Table 4-4, respectively.

Table 4-3 Measured fluoride and chloride contents of each of the melted slags.

	CMS-F (%)	CMS-N (%)	CMS-K (%)	CMS-SY (%)
Fluoride content	5.81	5.69	3.51	0.08
Chloride content	<0.1%	<0.1%	<0.1%	<0.1%

As was seen with the fluidizers, the fluoride content of the melted slags is somewhat less than would be present if no change in composition occurred. However, there is another important factor: much of the difference between expected and measured fluoride could be related to the weight loss at high temperatures, since fluorides tend to be more susceptible to volatilization than oxides. This relationship will be further discussed in section 4.5.

Table 4-4 Chemical analysis of metals in each of the melted slags. Metal contents were calculated as oxides.

	CMS-F (%)	CMS-N (%)	CMS-K (%)	CMS-SY (%)
Al_2O_3	0.2%	6.3%	8.0%	9.3%
CaO	49.8%	40.6%	44.4%	44.6%
Fe_2O_3	0.7%	0.1%	0.2%	0.7%
K_2O	<0.1%	0.1%	0.4%	0.1%
MgO	10.0%	11.2%	11.8%	12.7%
Na_2O	<0.1%	6.0%	<0.1%	0.2%
SiO_2	30.3%	33.1%	30.6%	31.6%
Total	91.0%	97.4%	95.4%	99.2%

The changes in composition of the slags during heating, with respect to metallic elements, may be seen in Table 4-4, particularly for the CMS-K slag. In this slag, the remaining potassium after heating is 0.4%, whereas prior to heating, it was 5.5% (based on a blended slag containing 20% $KAlF_4$). Similarly, the potassium initially present in the CMS-SY slag was almost entirely gone in the melted slag. This effect was not seen in the CMS-F slag, where the amount of calcium (evaluated as CaO) measured (49.8%) was almost exactly what was in the blended slag (50.3%). It was seen to a lesser extent in the CMS-N slag, where 8.9% Na_2O was expected based on the blended slag composition, and only 6.0% was measured in the melted product.

4.1.2 XRD

The XRD patterns for each of the fluidizers are shown in Figure 4.1, Figure 4.2, Figure 4.3, and Figure 4.4(showing CaF_2, Na_3AlF_6, $KAlF_4$, and spent salt, respectively), while Table 4-5 gives a summary of these results.
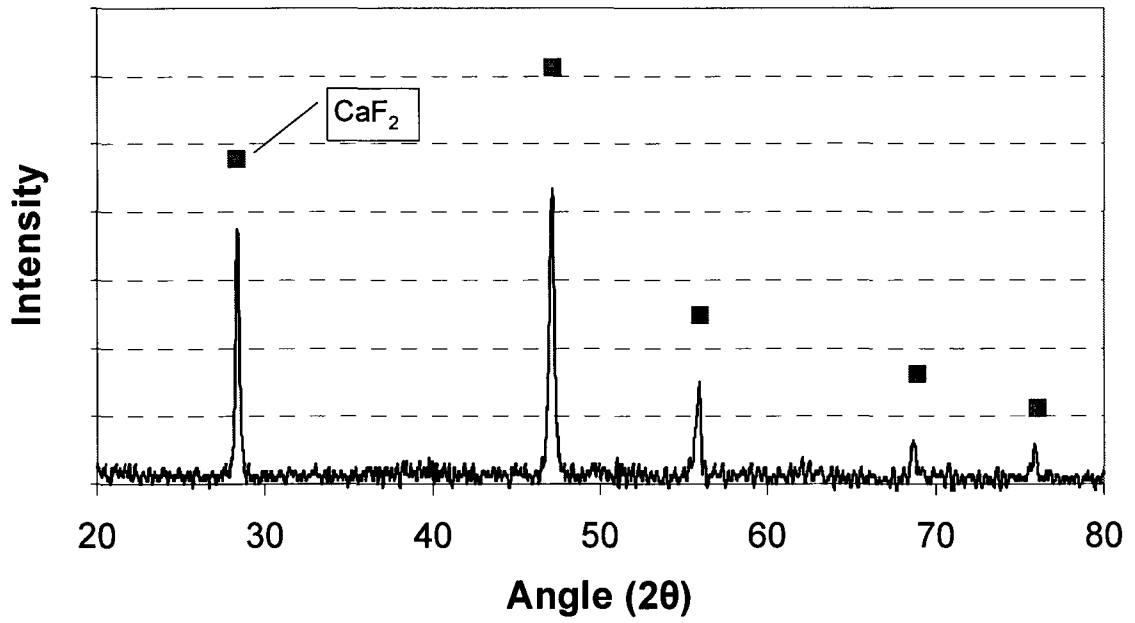
Figure 4.1 XRD pattern of CaF$_2$ fluidizer, showing peaks corresponding to CaF$_2$.
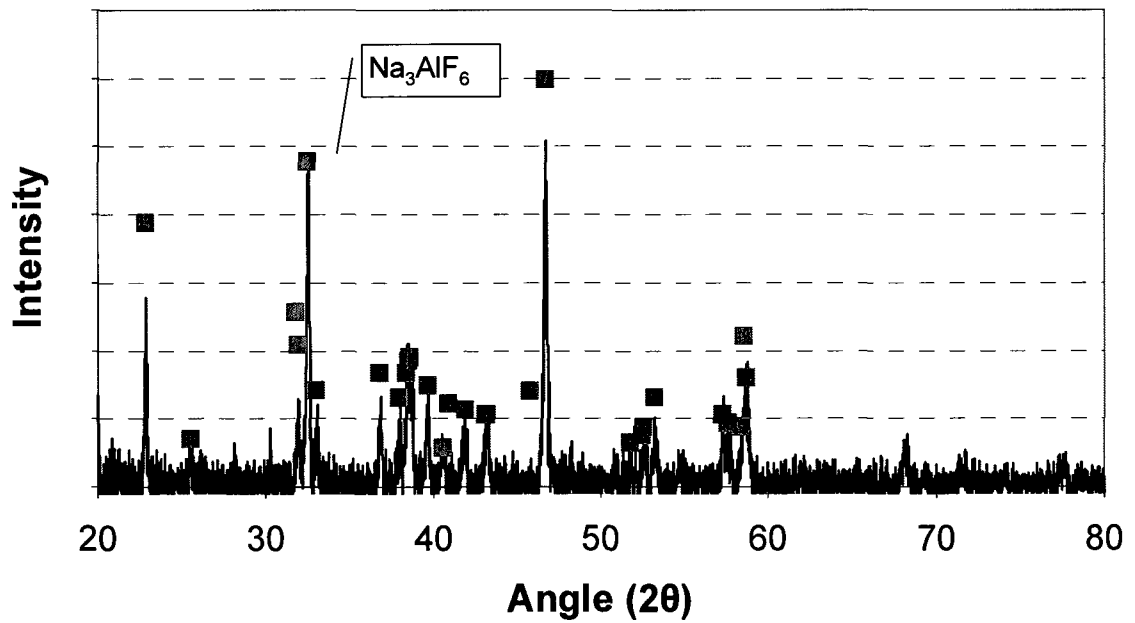
Figure 4.2 XRD pattern of Na$_3$AlF$_6$ fluidizer, showing peaks corresponding to Na$_3$AlF$_6$.
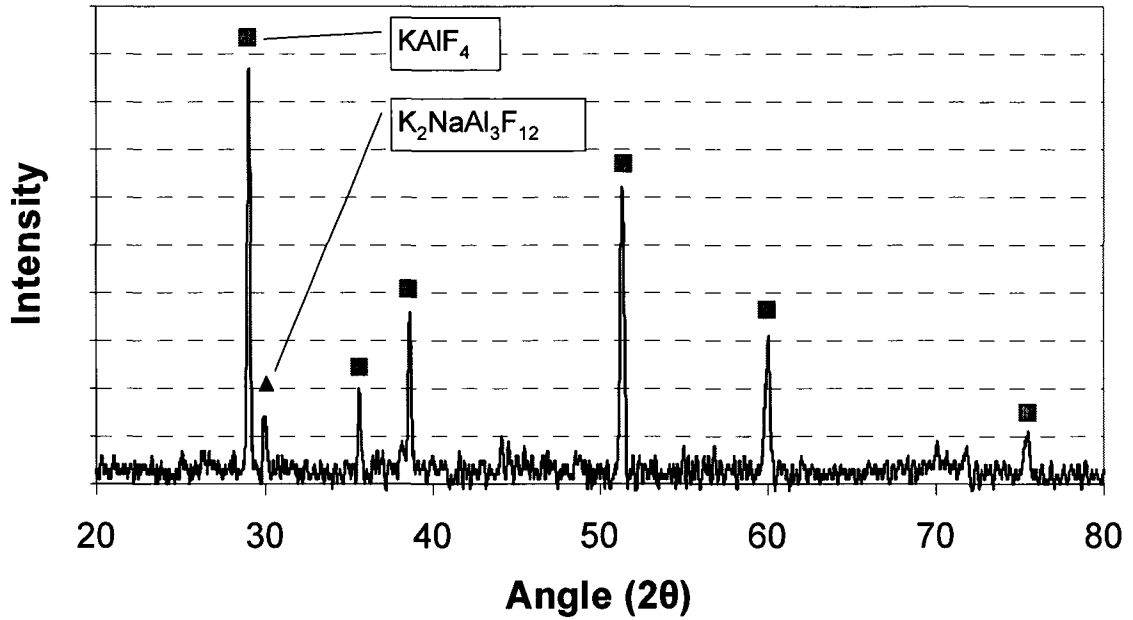
Figure 4.3 XRD pattern of KAlF₄ fluidizer, showing peaks corresponding to KAlF₄ and K₂NaAl₃F₁₂.
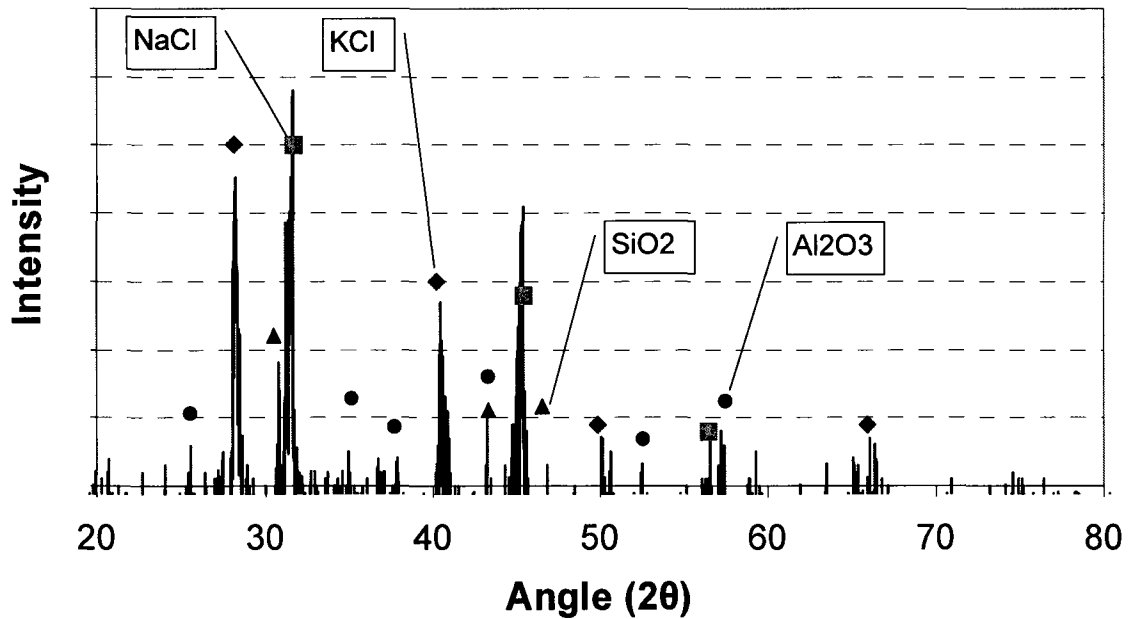
Figure 4.4 XRD pattern of spent salt fluidizer, showing peaks corresponding to NaCl, KCl, SiO₂, and Al₂O₃.

The XRD patterns for CaF_2 and Na_3AlF_6 showed only those phases, respectively. The

$KAlF_4$ pattern included a small amount of the $K_2NaAl_3F_{12}$ phase, though the very small

amount of sodium detected by ICP-OES is in apparent contradiction to this. Instead, it

may be possible that an atom of potassium is substituting for the sodium in the same

crystal structure as $K_2NaAl_3F_{12}$ to make "$K_3Al_3F_{12}$". Finally, the pattern for the spent salt

contained peaks for NaCl, KCl, Al_2O_3, and SiO_2, all of which were represented in the

analysis by ICP-OES. However, the major peaks were those of NaCl and KCl, while Al_2O_3

had relatively small peaks considering that it was the largest component in the material

as measured by spectroscopy. It is also surprising that no aluminum peaks were noted,

since there were visible particles of metallic aluminum in the unground spent salt. Either

Al_2O_3 or Al peaks should be more prominent, based on the chemistry of the material as

determined by ICP-OES.

Table 4-5 Summary of phases detected by XRD for slag fluidizers.

	CaF_2	Na_3AlF_6	$KAlF_4$	Spent salt
Phases detected	CaF_2	Na_3AlF_6	$KAlF_4$, $K_2NaAl_3F_{12}$	NaCl, KCl, Al_2O_3, SiO_2

The XRD patterns for each of the melted slags are shown in Figure 4.5, Figure 4.6, Figure

4.7, and Figure 4.8(showing CMS-F, CMS-N, CMS-K, and CMS-SY, respectively), and a

summary of these results is shown in Table 4-6. It is important to note that the CMS-K

slag was seen to have a glassy appearance in the fastest-cooled region, unlike the other

slags. Any amorphous or glassy material would be expected to be detrimental toward

examining the material through XRD, though there was still some crystalline material found upon testing the entire sample.
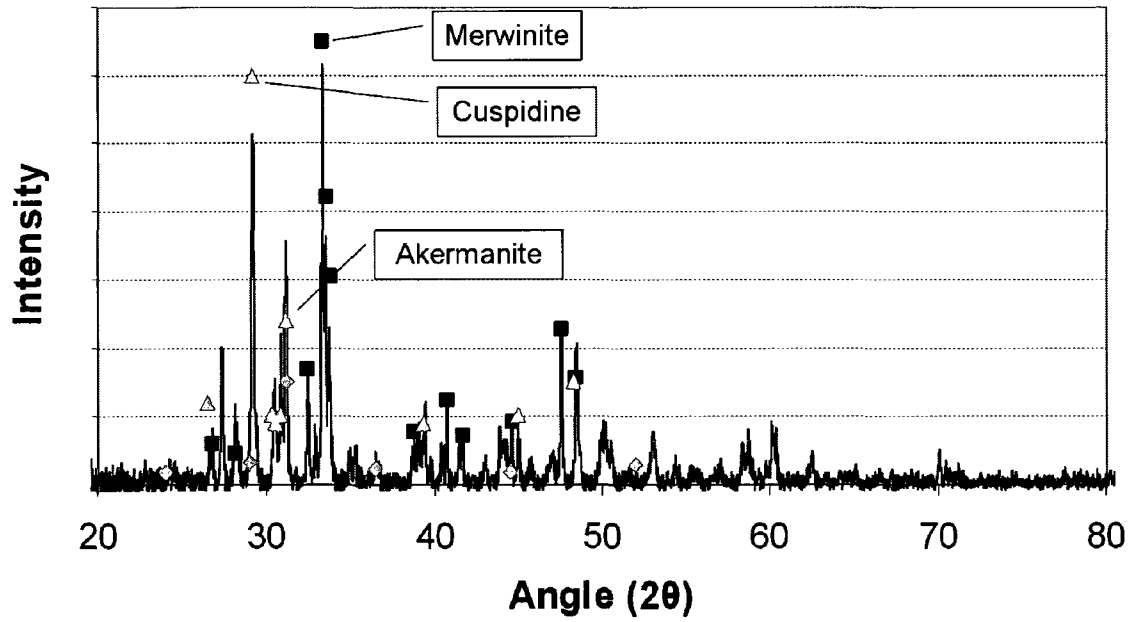
Figure 4.5 XRD pattern of melted CMS-F slag, showing peaks corresponding to merwinite, cuspidine, and akermanite.
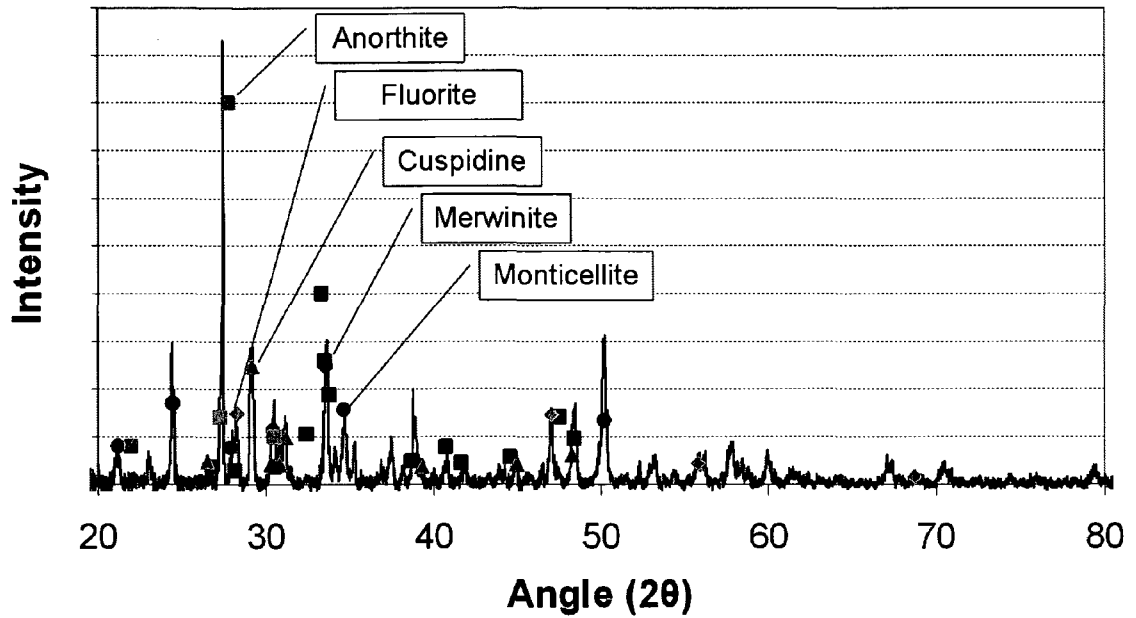
Figure 4.6 XRD pattern of melted CMS-N slag, showing peaks corresponding to anorthite, merwinite, cuspidine, fluorite, and monticellite.
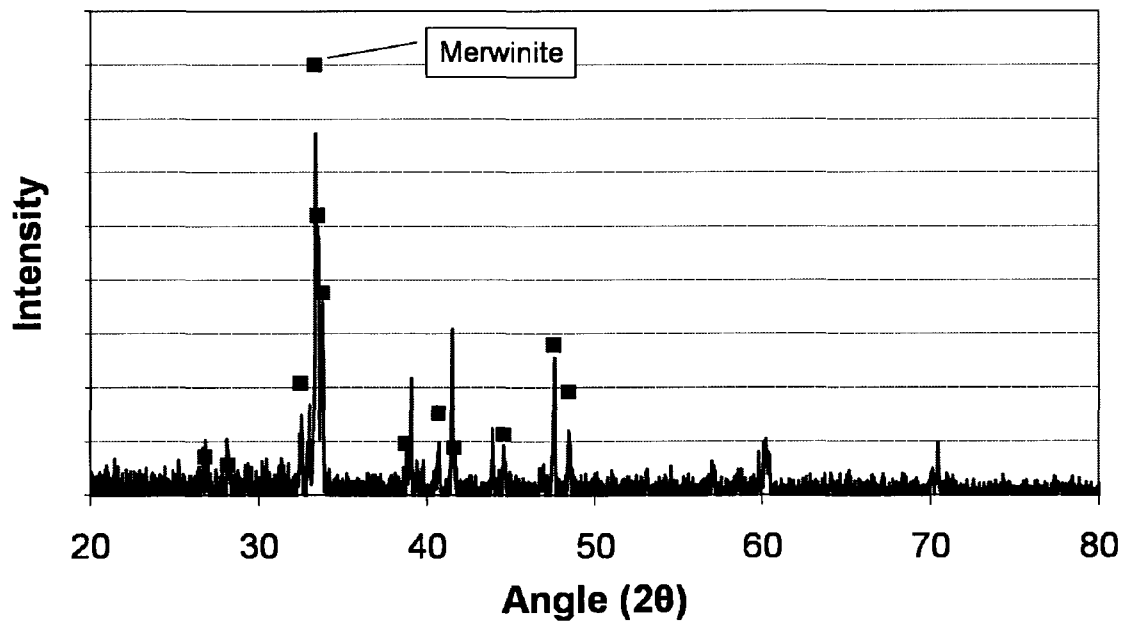
Figure 4.7 XRD pattern of melted CMS-K slag, showing peaks corresponding to merwinite.
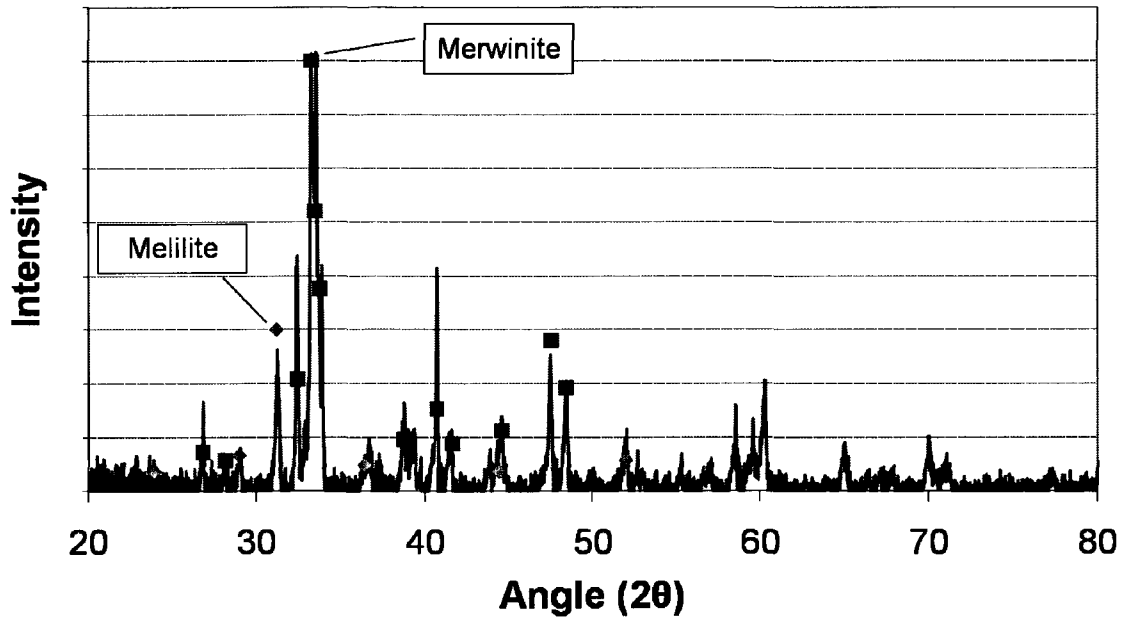
Figure 4.8 XRD pattern of melted CMS-SY slag, showing peaks corresponding to merwinite and melilite.

The phases found through XRD were, with the exception of fluorite, silicate phases. The absence of more refractory phases (such as CaO, MgO, Al_2O_3, or spinels) is notable from the viewpoint of viscometry, since any of these would be solid at steelmaking temperatures and therefore increase the viscosity greatly. These measurements also agree with the phases calculated to be present (as shown in Table 4-8) or those examined by EPMA (as shown in Table 4-9) to a large extent. Merwinite is the only phase to appear in each of the patterns, but is significantly reduced in intensity in the CMS-N slag, indicating that anorthite is possibly the primary phase formed.

Table 4-6 Summary of phases detected by XRD for melted slags. Compositions of the minerals are given in Table 4-9.

	CMS-F (%)	CMS-N (%)	CMS-K (%)	CMS-SY (%)
Phases detected	Merwinite, cuspidine, akermanite	Anorthite, merwinite, cuspidine, monticellite, fluorite	Merwinite	Merwinite, melilite

4.2 VISCOMETRY

4.2.1 VISCOMETER CALIBRATION

The viscometer was calibrated using silicone oils of known viscosity. The oils used had viscosities of 240 cP, 490 cP, 975 cP, and 4820 cP and were supplied by Brookfield Engineering. Each oil was tested, at 30 rpm, with an MgO crucible and Al_2O_3 spindle of the same type as was used for viscosity testing. The results of the calibration tests are plotted in Figure 4.9. The viscometer signal was a voltage proportional to the torque used to turn the spindle, and since the oils were considered to be Newtonian, measurements at a constant speed of these fluids yielded a linear result. A small amount of cyclic error was inherent in each measurement, due to "wobbling" of the spindle around the centre point of the crucible. This produced a sinusoidal signal in all media tested.
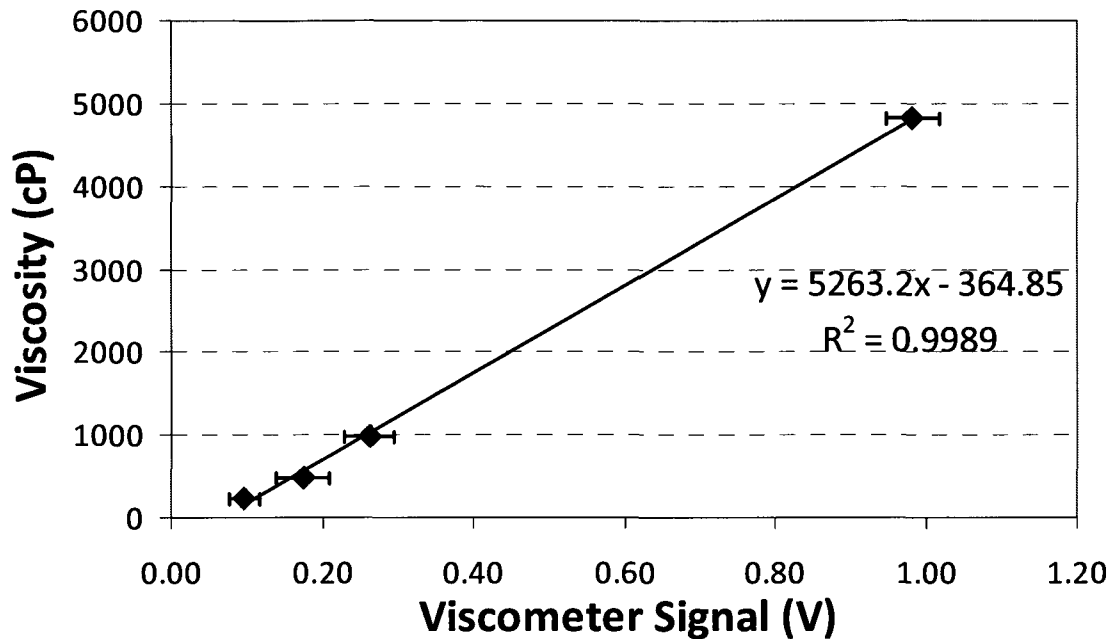
Figure 4.9 Plot of viscosity vs. viscometer signal for 4 standard silicone oils used for calibration of the viscometer at 30 rpm, and fitted line used for interpreting measurements.

4.2.2 COMPARISON WITH PRIOR WORK

Viscometry results using the first slag, CMS-F (containing 20% CaF_2), were compared to prior viscometry work done using the same equipment and composition. Viscometry results for this slag, as recorded by several researchers, are shown in Figure 4.10. This figure illustrates the very good correlation between three of the four curves in terms of the temperature of transition (about 1310 °C) between low viscosity and high viscosity regions. Also, the absolute values of viscosity observed above this transition temperature are within approximately 175 cP, which is nearly within the expected error found during calibration of the viscometer.
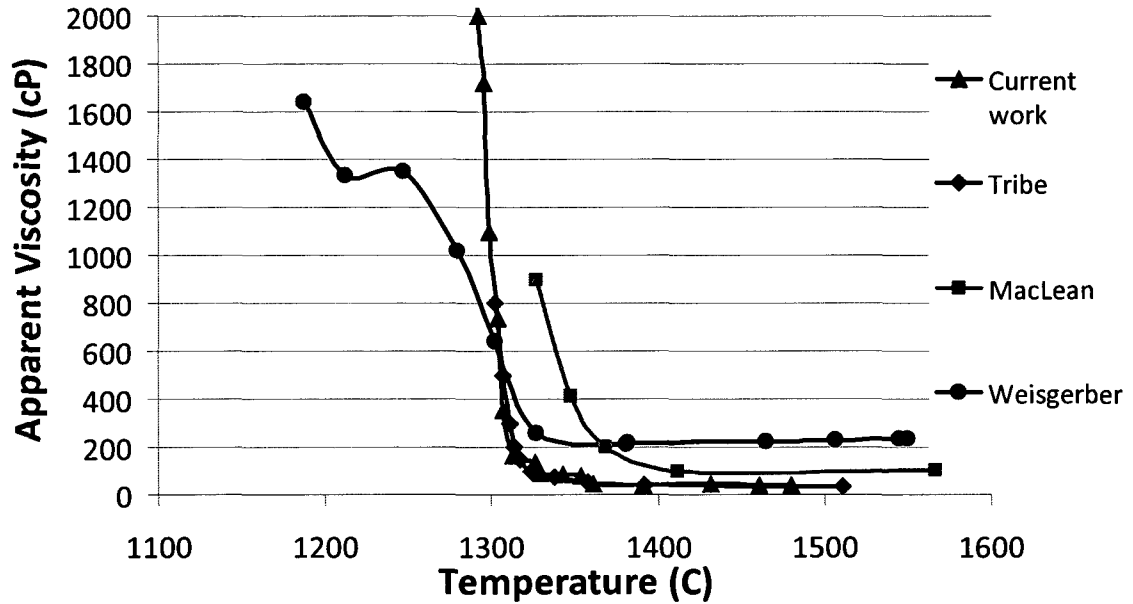
Figure 4.10 Comparison of current work using CMS-F slag with past apparent viscometry results[22,23,24].

4.2.3 REPRODUCIBILITY OF RESULTS

To ensure that the viscosity tests done were repeatable, each of the tests was duplicated. An example of a duplicate test, once again using the CMS-F slag, is shown in Figure 4.11. Figure 4.10 and Figure 4.11 show that the reproducibility of these tests is therefore possible to within about 50 °C (in terms of transition from low to high viscosity) and 175 cP (at the highest temperatures).
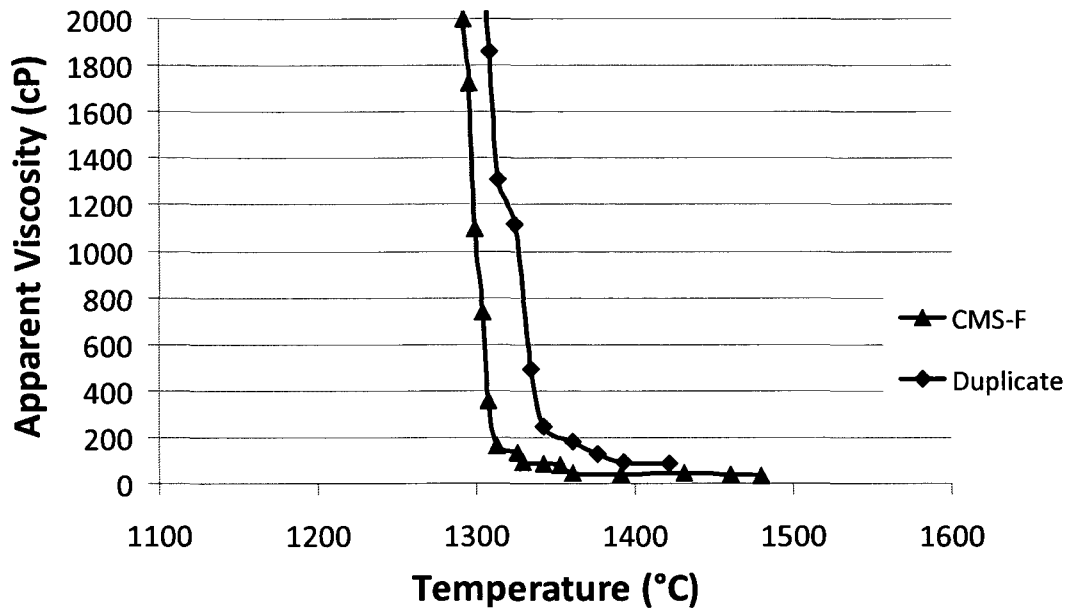
Figure 4.11 Comparison of duplicated apparent viscosity tests, using CMS-F slag.

4.2.4 SLAG VISCOSITY MEASUREMENTS

Apparent viscosity-temperature curves were obtained for each of the slags tested. The results are shown in Figure 4.12, Figure 4.13, Figure 4.14, and Figure 4.15, which correspond to the 4 slags: CMS-F, CMS-N, CMS-K, and CMS-HC, respectively.
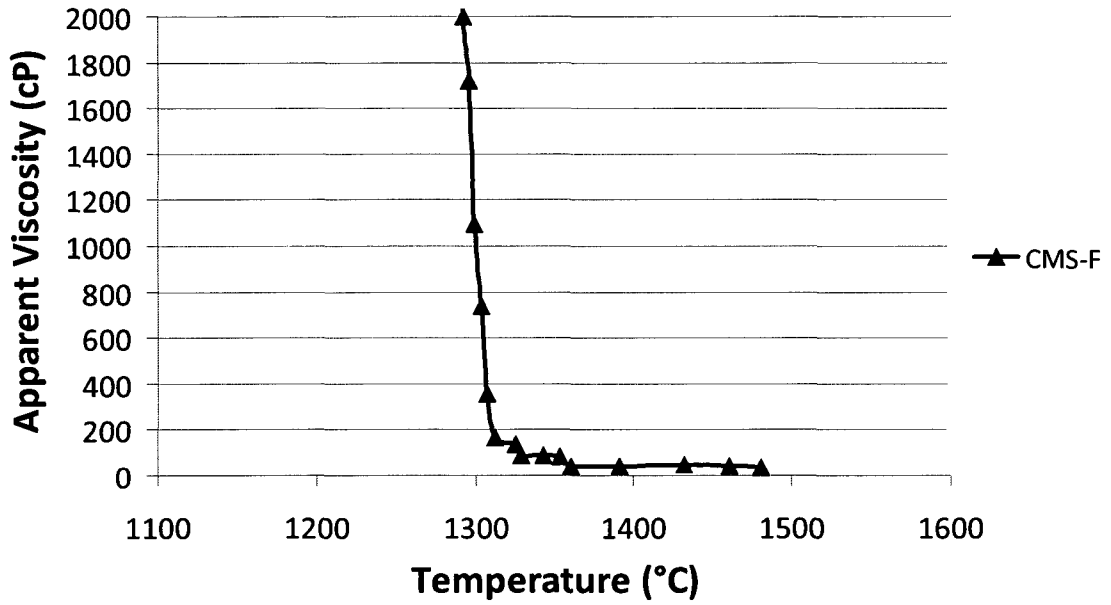
Figure 4.12 Apparent viscosity measurement for the CMS-F slag.
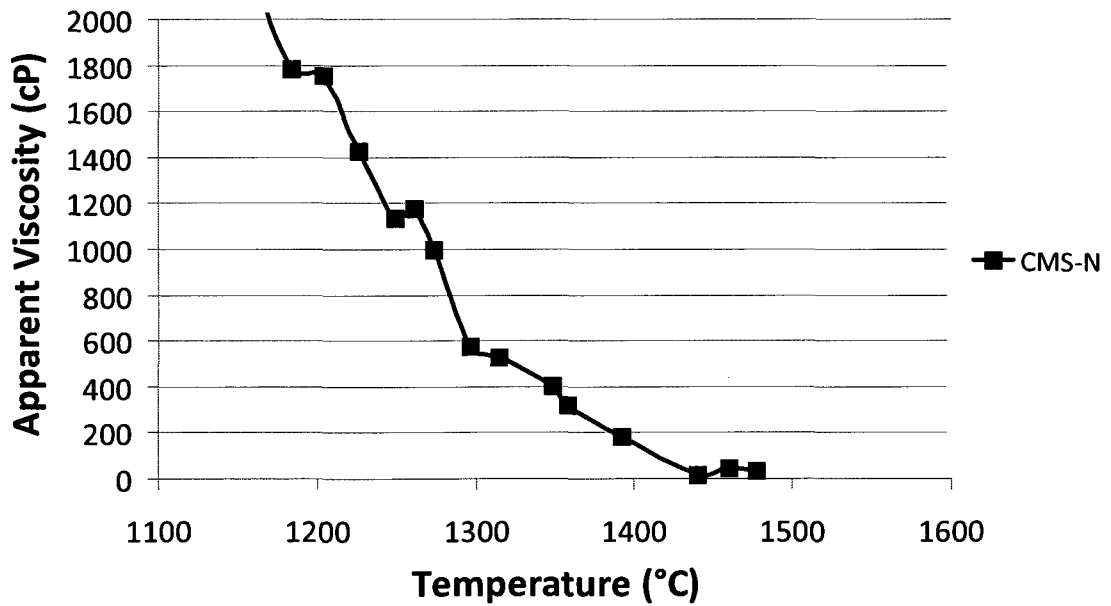
Figure 4.13 Apparent viscosity measurement for the CMS-N slag.
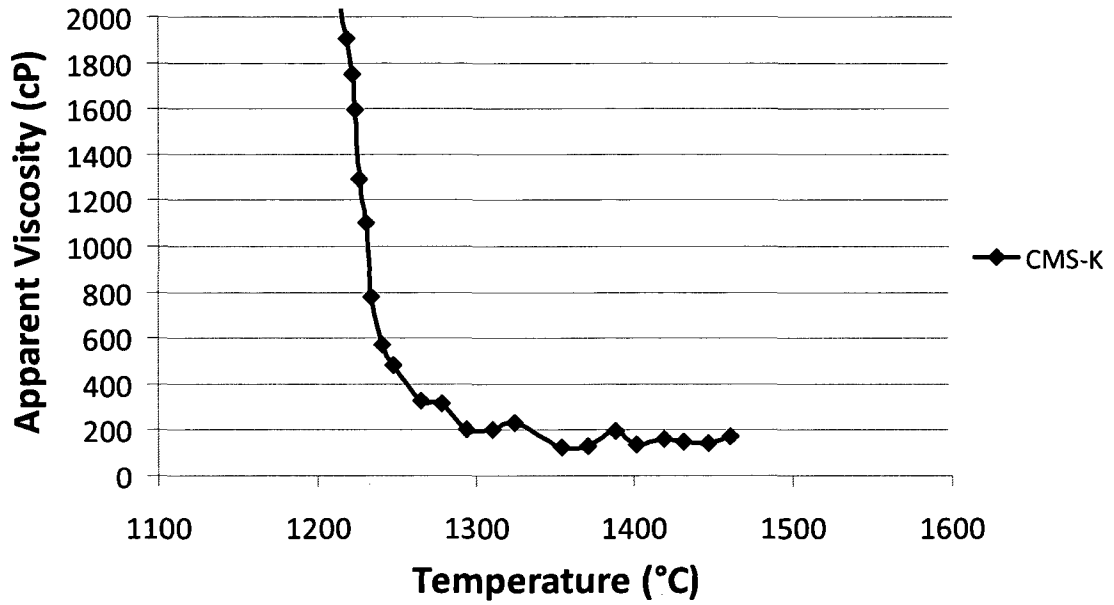
Figure 4.14 Apparent viscosity measurement for the CMS-K slag.
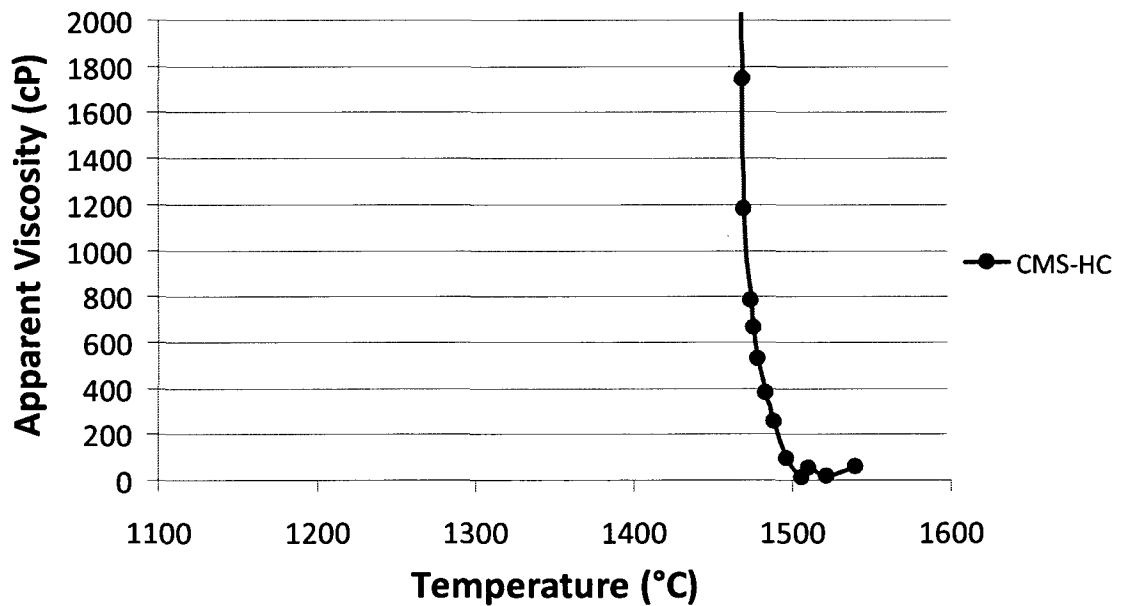
Figure 4.15 Apparent viscosity measurement for the CMS-HC slag.

There were a few clear differences between the slags, best illustrated by Figure 4.16. First, the slag containing Na_3AlF_6 showed a much more gradual transition from high to low apparent viscosity than the rest, indicating a more acidic structure than the other slags. The temperatures at which this transition occurred was also different for each slag: 1500 °C for CMS-HC, 1435 °C for CMS-N, 1310 °C for CMS-F, and 1260 °C for CMS-K. It is important to note that all of these temperatures are somewhat below typical steelmaking temperatures, meaning that the slags would be fluid in steelmaking operations. Also, the slags tested all exhibited apparent viscosity between 40 and 200 cP at high temperatures, which is an appropriate range of viscosity for steelmaking slags.
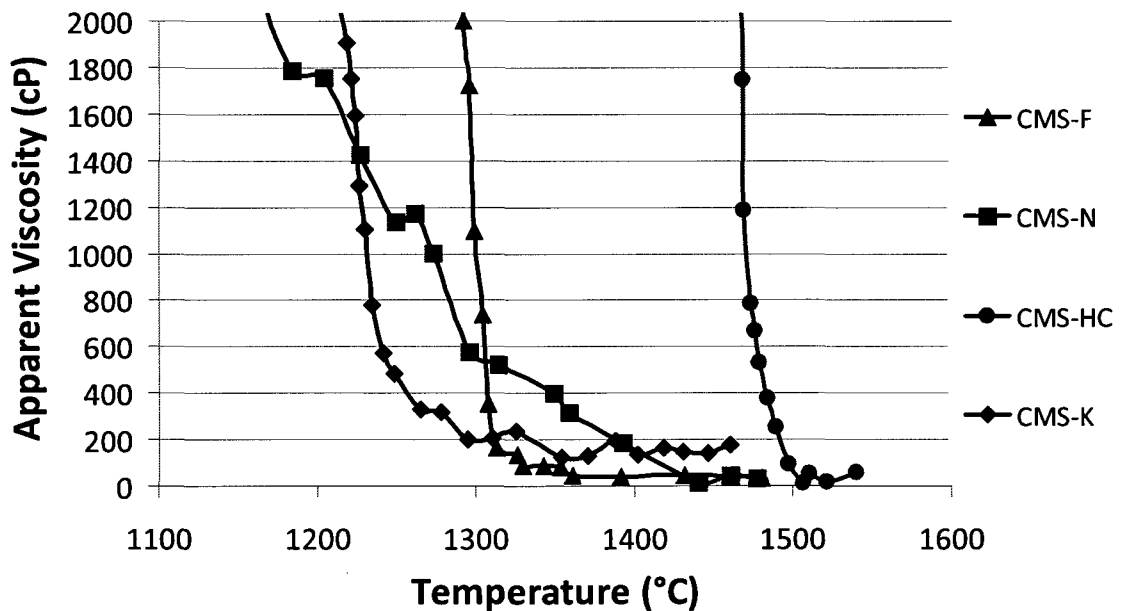
Figure 4.16 Comparison of apparent viscosity of slags containing different fluidizers.

4.2.5   OTHER OBSERVATIONS

During testing, a number of other observations were made about the slags, particularly the CMS-N slag. A yellow-orange flame was observed emanating from the furnace when this slag was heated for viscosity testing, and a film of dust was found to have formed on cooler parts of the spindle and the viscometer after testing. This further reinforces the fact that there was significant vaporization of sodium compounds (which typically burn with a yellow flame) from the melt. Also in this slag, the spindle had a strong tendency to stick to the sides of the crucible if it was improperly aligned.

After sectioning, it was seen that the CMS-HC slag contained some porosity near the surface of the liquid, which could have been caused by bubbles of gas forming throughout the melt. There were also small grains of visible metal near the bottom of the crucible. Finally, there was some visible thinning of both the crucible and spindle at the slag line in all of the slags, indicating some reaction and dissolution of both MgO and Al_2O_3.

4.3   WEIGHT LOSS TESTING

4.3.1   WEIGHT LOSS MEASUREMENTS

The amount of weight lost by each slag is shown in Figure 4.17. The measurements were normalized to 600 °C, meaning that the weight at 600 °C was treated as the initial weight. The results show that the CMS-F slag lost less than 1% of its mass, even at the

highest temperature, while the other three slags had significantly more mass lost at all temperatures. The CMS-SY slag shows an interesting result: much of the weight is lost below 1100 °C, and nearly none was lost above this temperature.
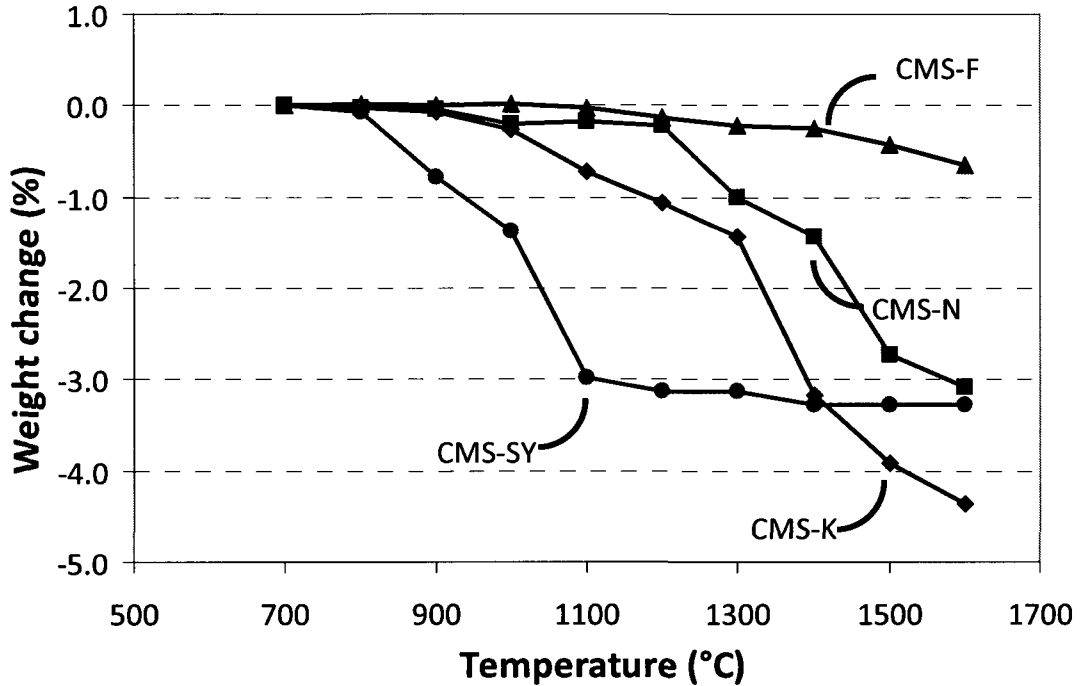
Figure 4.17 Weight loss measurements, normalized to 600 °C.

4.3.2 THERMODYNAMIC CALCULATIONS

As a method of comparison and verification of the results obtained from weight loss experiments, thermodynamic calculations of the amount of gas in the system were performed using the FACTSage 6.1 software package. These calculations were done in increments of 10 °C for each of the slag compositions chosen, using data from the FToxid and FACT53 databases. In addition, the amounts of liquid and solid phases (given a mass of 100 g of slag at room temperature) formed in each system at each

temperature were determined to evaluate any effects that this might have on the rheology of the system. For each slag, the calculated amount of weight change is shown in Figure 4.18 and the calculated amount of liquid formed is shown in Figure 4.19.
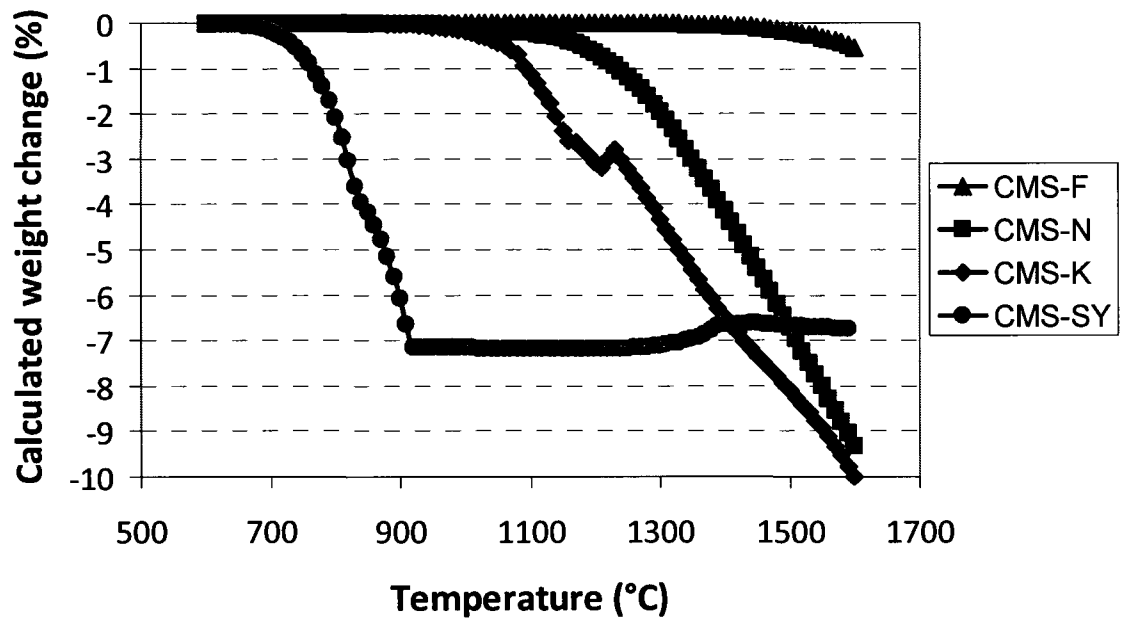
Figure 4.18 Calculated weight change upon heating of each slag in an excess of oxygen.

The measured and calculated weight changes have much in common. The shape and order (CMS-F losing the least weight at the highest temperature, followed by CMS-SY, CMS-N, and CMS-K) of the curves were well matched. The one discrepancy to note in the CMS-N, CMS-K, and CMS-SY slags was the magnitude of the weight loss: the largest weight loss measured was less than 5%, while the calculations predicted a loss of nearly 10% (both for the CMS-K slag). With the CMS-F slag, there was nearly perfect agreement between the calculated and measured curves, showing a final weight loss of about 0.5% in both cases. The CMS-SY slag showed the predicted behaviour of higher weight loss at

lower temperatures, though this weight loss only stopped at 1100 °C rather than at 900 °C as was calculated.

The major components of the gas phase calculated for each slag are shown in Table 4-7. It is clear that halides and alkali metals were the most likely to go into the gas phase, as no oxides were calculated to volatilize in any measurable amount and the alkali halides were the largest contributors to the gas phases in the CMS-N, CMS-K, and CMS-SY slags. It is interesting, though, that one of the more common fluoride phases that has been found to volatilize from slags is SiF_4[31,32], which is only seen here in the CMS-K slag.

Table 4-7 Calculated gas phase components for each slag, listed in descending order by mass.

	CMS-F	CMS-N	CMS-K	CMS-SY
Calculated gas phase components	CaF_2, MgF_2	NaF, CaF_2, MgF_2, $NaAlF_4$, $(NaF)_2$	KF, CaF_2, MgF_2, AlF_3, SiF_4	NaCl, KCl, Cl

The amounts of liquid calculated to be present is one method of estimating the viscosity of a basic melt; as the solids content approaches zero, the viscosity should decrease quickly toward a low (100-500 cP) viscosity. This behaviour can be described by equation (6). The amount of liquid calculated to be present in the CMS-F slag, for example, approaches 100 g at approximately 1310 °C, which is the transition temperature from fluid to viscous in this slag. The CMS-K slag shows a similar relationship, with a transition temperature of 1260 °C corresponding to no calculated solids at approximately the same temperature. This correlation is not as accurate for the

other slags, however: the transition temperatures for the CMS-N and CMS-HC slags are both much higher than would be predicted by this method (275 °C higher in the former case, and 50 °C higher in the latter).
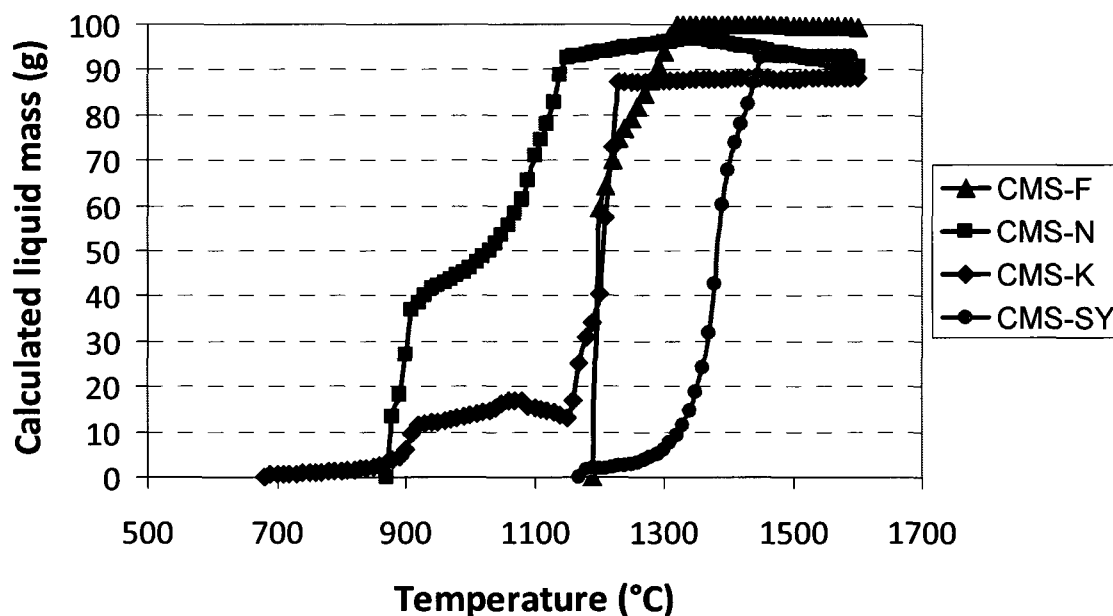
Figure 4.19 Calculated amount of liquid present in each slag when heated in an excess of oxygen.

The solid phases calculated to form upon freezing of each slag are shown in Table 4-8. The only differences between the phases shown in XRD and those present in the calculations are anorthite in CMS-N (which takes the place of the calculated combeite and NaAlO$_2$, and is similar in composition), the lack of phases except for merwinite shown by XRD in the CMS-K slag (which may be attributed to the glassy phase formed during cooling of the slag), and the calculated spinel phase which was not found in the CMS-SY. Both XRD results and the calculated phases will be discussed further in section 4.4.1, in comparison to the mineralogy of the samples as determined by EPMA.

Table 4-8 Solid phases calculated to form on cooling of slags.

	CMS-F	CMS-N	CMS-K	CMS-SY
Calculated solid phases on cooling	Merwinite, cuspidine, akermanite	Merwinite, monticellite, fluorite, combeite ($Na_2Ca_2Si_3O_9$), $NaAlO_2$	Merwinite, monticellite, akermanite, fluorite, kaliophilite ($KAlSiO_4$), gehlenite	Merwinite, akermanite, gehlenite, spinel

4.4 EPMA

Two sets of points and images were obtained: those examining the bulk of the slag away from the spindles and crucibles, and those examining the interactions between the slag and the crucibles and spindles. The ideal compositions of the mineral phases found in the slags are shown in Table 4-9.

Table 4-9 Mineral phases found in slags and refractories used for viscometry[21].

Name	Composition	Liquidus Temperature (°C)
Alumina	Al_2O_3	2020
Magnesia	MgO	2764
Spinel	$MgO{\cdot}Al_2O_3$	2135
Merwinite	$3CaO{\cdot}MgO{\cdot}2SiO_2$	1575
Monticellite	$CaO{\cdot}MgO{\cdot}SiO_2$	1490
Dicalcium silicate	$2CaO{\cdot}SiO_2$	1544
Cuspidine	$3CaO{\cdot}CaF_2{\cdot}SiO_2$	1407
Gehlenite	$2CaO{\cdot}Al_2O_3{\cdot}SiO_2$	1596
Akermanite	$2CaO{\cdot}MgO{\cdot}2SiO_2$	1436
Melilite	Solution of gehlenite-akermanite	Dependent on composition
Variable alkali calcium aluminosilicates	K_2O or Na_2O + CaO + Al_2O_3 + SiO_2	Dependent on composition

4.4.1 BULK SLAG MINERALOGY

Figure 4.20, Figure 4.21, Figure 4.22, Figure 4.23, Figure 4.24, and Figure 4.25 show the structures and mineralogical make-up of the 4 slags used. One image is shown of each of the CMS-F, CMS-N, and CMS-K slags, while the images of the CMS-HC slag show three distinct regions within the bulk. The numerical results of the EPMA analysis are listed in Appendix C, both by weight percent and by atomic percent. For simplicity, the discussion will only consider weight percent.

The analysis for the CMS-F slag, shown in Figure 4.20, indicated 3 phases: dicalcium silicate (containing approximately 0.5% fluorine), merwinite, and monticellite. The total weight percent found in the analysis for point 1 was only 93.75%, indicating that there is a missing component of the phase. It is likely that much of this missing weight is fluorine, for four reasons.

The first reason is that the amount of fluorine in the slag (as-mixed) should be 9.7%, and the only fluorine found was 0.5% of one phase, while the fluorine content of the melted slag as shown in section 4.1.1 was 5.81%. Secondly, the mass was not lost through simple heating in the furnace, since it was shown in section 4.3.1 that this type of slag only lost approximately 0.5% of its weight, not nearly enough to account for the discrepancy. Thirdly, it is possible for materials to be strongly degraded by the electron

beam while EPMA is being done. If this occurred to cuspidine, and most of the fluorine was removed by the electron beam, then the remnant phase would resemble dicalcium silicate with some residual fluorine, and the total amount of material counted would be lower. Finally, the cuspidine phase (and not dicalcium silicate) was a major peak that was detected in XRD. Because of this, it is believed that this phase was cuspidine which was degraded by the electron beam. This conclusion was carried through to occurrences of cuspidine in the other slags, since they exhibited the same type of chemistry.

It is surprising, though, that akermanite was not detected in this sample, since it was both detected by XRD in the same slag and predicted by the thermodynamic calculations. Instead, monticellite was found, which could have been a result of local CaO diffusion in the slag.
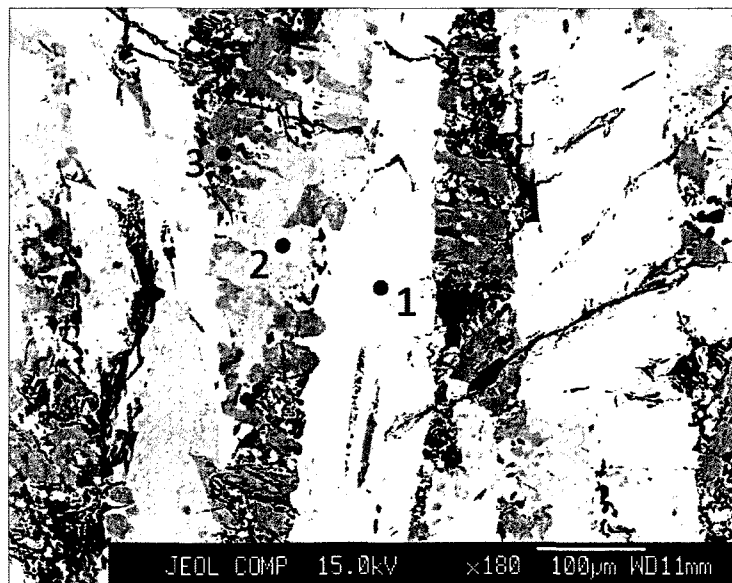
Figure 4.20 Backscattered electron image and chemical analysis points of CMS-F slag away from crucible and spindle. 1=cuspidine, 2=merwinite, 3=monticellite.

The CMS-N slag (Figure 4.21) was found to contain 3 phases in the bulk: cuspidine, monticellite, and a sodium-rich calcium aluminosilicate. Some fluorine was contained in the cuspidine as well as the Na-rich calcium aluminosilicate. In composition, the latter phase somewhat resembled anorthite, which was detected by XRD, but also contained some magnesium, which is not a normal constituent of anorthite. As well, merwinite (which was predicted by thermodynamic calculations) was not located by EPMA, though detection by XRD confirms its presence.
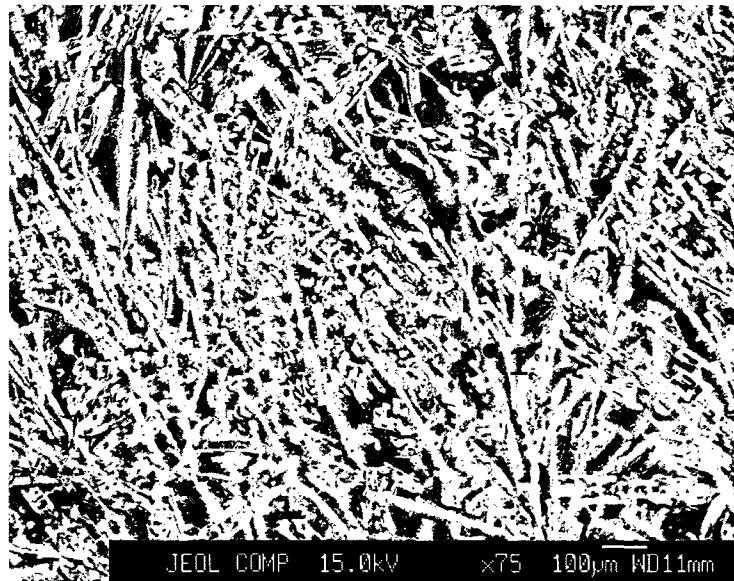
Figure 4.21 Backscattered electron image and chemical analysis points of CMS-N slag away from crucible and spindle. 1=cuspidine, 2=monticellite, 3=Na-rich alkali calcium aluminosilicate.

There were three phases found in the CMS-K slag: merwinite, cuspidine, and a potassium-rich calcium aluminosilicate. The latter two phases contained fluorine. Once again, the former two phases were expected, and the third was seen as $KAlSiO_4$ in

calculations. Monticellite, akermanite, gehlenite, and fluorite were also anticipated, though, and not found in the bulk of the sample, which is shown in Figure 4.22.
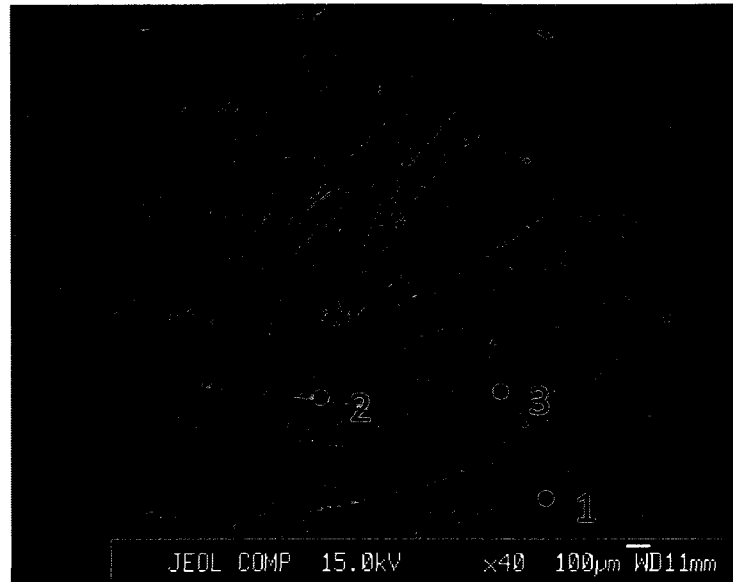
Figure 4.22 Backscattered electron image and chemical analysis points of CMS-K slag away from crucible and spindle. 1=merwinite, 2=cuspidine, 3=K-rich alkali calcium aluminosilicate.

The bottom part of the CMS-HC slag, shown in Figure 4.23 was a slightly porous mass that otherwise largely resembled the other slags, with the notable absence of cuspidine (since there was little fluorine in this slag). The phases present were merwinite, monticellite, and melilite. In one instance, a melilite grain contained 4.1% chlorine. Monticellite was not one of the phases predicted by calculations, and spinel, which was predicted, was not observed.
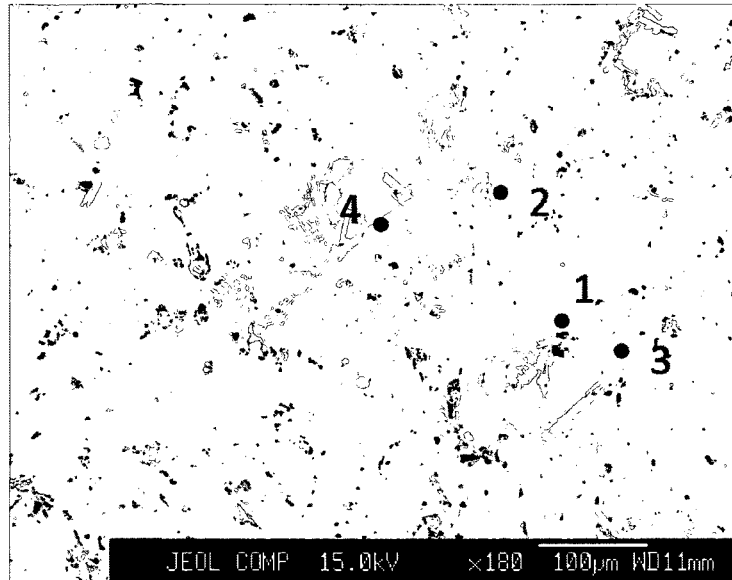
Figure 4.23 Backscattered electron image and chemical analysis points of CMS-HC slag away from crucible and spindle, in the lower part of the melt. 1=merwinite, 2=monticellite, 3=melilite, 4=melilite (containing chlorine).

Figure 4.24 shows an image of the porous top part of the CMS-HC slag. Only two phases were detected here: melilite and monticellite. There appeared to be a liquid formed on the sample during imaging; a slightly irregular droplet can be seen in this image, above point 1. This liquid could be residual fluid from polishing, since the porous surface would allow the polishing fluid to enter the sample. The droplet could be seen moving as the beam was focussed near it, but for fear of damaging the equipment, chemical analysis was not done, as a relatively long beam dwell time over a potentially volatile substance could boil or evaporate the liquid, causing problems in the column.
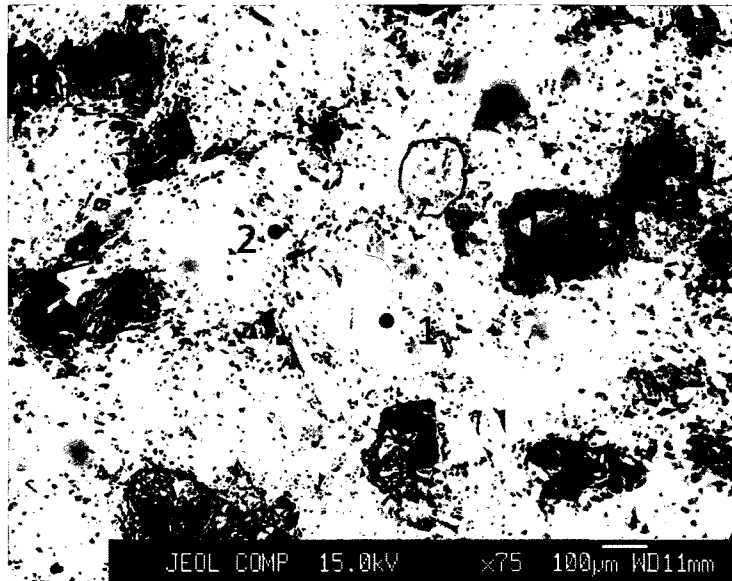
Figure 4.24 Backscattered electron image and chemical analysis points of CMS-HC slag away from crucible and spindle, in the upper part of the melt. 1=melilite, 2=monticellite.

Figure 4.25 shows an image of a metallic droplet near the bottom of the CMS-HC slag. This droplet, when analyzed, showed a total weight percent measurement of 16.1%, meaning that the large majority of the metal drop's composition was an element (or elements) that were not being examined. Those elements being tested were Al, Ca, Cl, F, K, Mg, Na, O, and Si, and the only elements detected in amounts greater than 1% were Al (11.8%), Si (3.2%), and O (1.1%). Since the only other element detected by ICP-OES in a significant amount in the spent salt material was Fe, it is very likely that the metal droplet was primarily iron. The content of aluminum, silicon, and oxygen may be misleading as well, since any WDS peak overlaps of these elements with iron would not have been accounted for in the calibration process. It is also very unlikely that iron with a high aluminum and silicon content would contain as much as 1.1% oxygen, as the Al and Si would serve to deoxidize the liquid alloy.

The other phases detected in this image were melilite and monticellite, which is consistent with the other parts of the slag. A circular droplet of liquid was observed next to point 2. Again, it is suspected that this liquid was present in the pores of the sample from polishing.
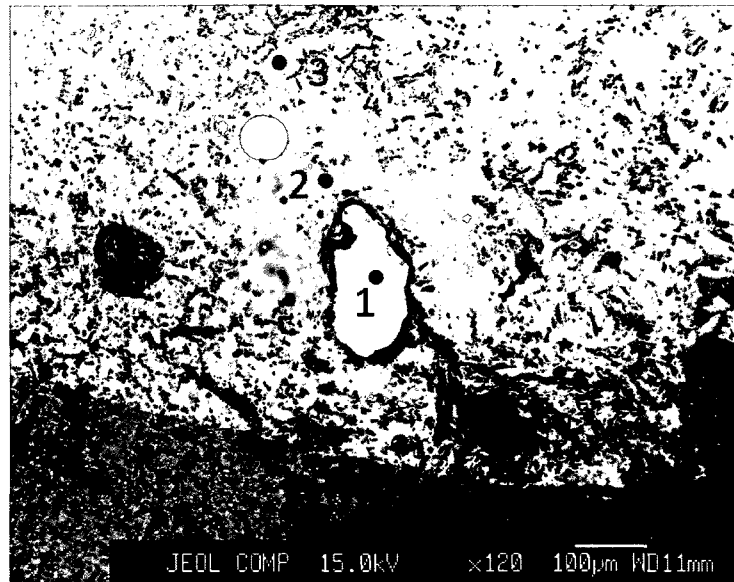
Figure 4.25 Backscattered electron image and chemical analysis points of CMS-HC slag, showing metallic particle (point 1) near the bottom of the crucible. 1=Fe-Al-Si alloy, 2=melilite, 3=monticellite.

4.4.2 CORROSION OF SPINDLE AND CRUCIBLE

Analysis of the slags near the spindle and crucible was undertaken in order to quantify the corrosion of refractory materials by the slags used. The phases observed were of the same types as those in the bulk of the slag, though some contained higher amounts of refractory constituents due to dissolution of the crucible or spindle.

Figure 4.26 shows the region of the spindle in the CMS-F slag. Four phases appear to be functional in attacking the spindle: alumina (the spindle itself), cuspidine, gehlenite, and spinel. Alumina was apparently dissolved in the slag and precipitated out into a spinel phase a short distance away from the spindle. This creates a small layer of gehlenite and cuspidine (both magnesia-depleted phases) between the solid alumina and a loose layer of spinel. Beyond the layer of spinel, the slag has essentially the bulk composition once again, showing monticellite and cuspidine in this instance. Corrosion in this instance does not extend an appreciable distance in the non-porous alumina.
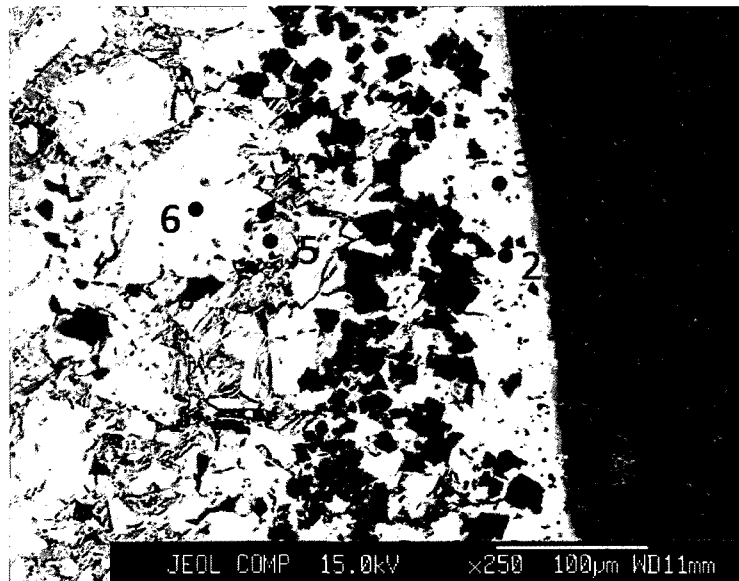
Figure 4.26 Backscattered electron image and chemical analysis points of CMS-F slag near the spindle. 1=alumina, 2=cuspidine, 3=gehlenite, 4=spinel, 5=monticellite, 6=cuspidine.

Figure 4.27 and Figure 4.28 are images of the CMS-F slag in contact with the MgO crucible wall. In this case, the wall appeared discoloured where it was affected by the

slag. As well, there is a layer of slag built up along the crucible that was analyzed to be

cuspidine containing some magnesium. Beyond this layer, the slag appears to be the

same as the bulk. Figure 4.28 shows a closer view of the affected region of the crucible,

where analysis was done on an MgO grain, and on the lighter phase that penetrated

into the crucible. Chemically, this second phase was cuspidine containing some

magnesia. Both of these images indicate some dissolution of the refractory into the

cuspidine phase, meaning that there is some significant damage to the crucible as well

as simple infiltration by liquid slag.
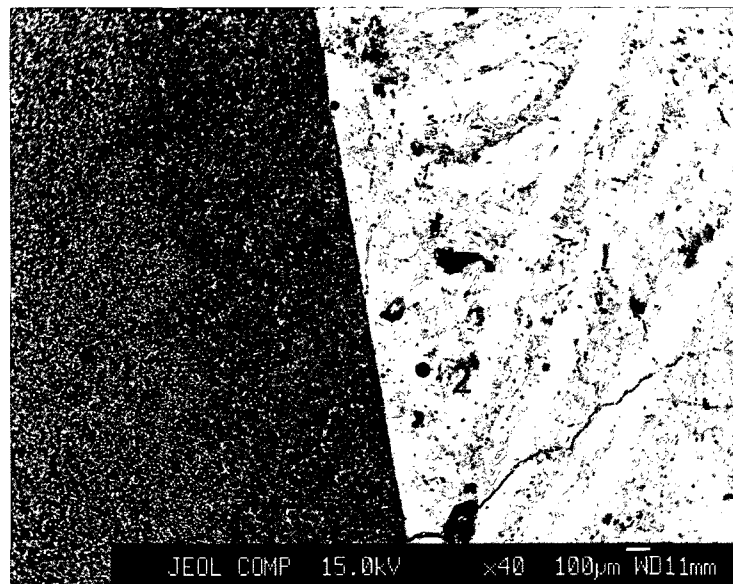
Figure 4.27 Backscattered electron image and chemical analysis points of CMS-F slag near the crucible. 1=magnesia, 2=cuspidine (containing magnesium).
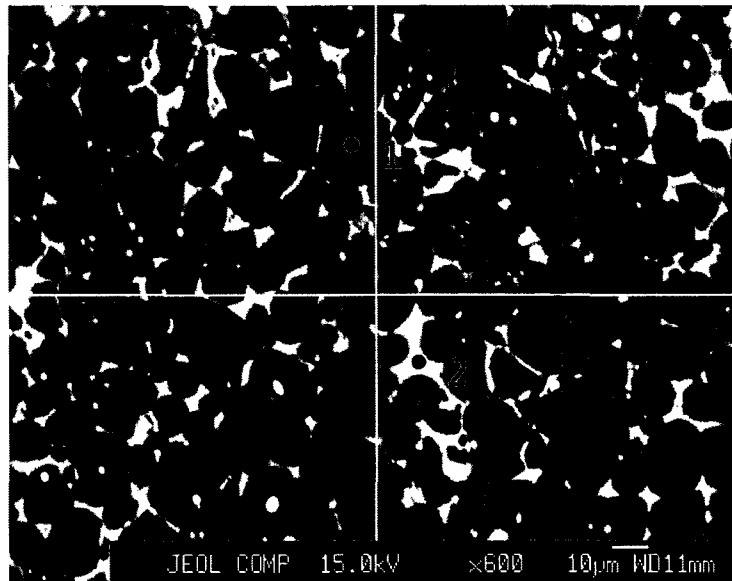
Figure 4.28 Backscattered electron image and chemical analysis points of crucible containing CMS-F slag, showing MgO grains (point 1) and penetrating slag (point 2). 1=magnesia, 2=cuspidine (containing magnesium).

The region surrounding the spindle in the CMS-N slag is shown in Figure 4.29. A thin layer of spinel is seen immediately next to the alumina spindle, beyond which the composition of the slag is the same as the bulk. This indicates that less corrosion occurred as compared with the CMS-F, likely due to the higher amount of alumina already contained within the CMS-N slag (meaning that less alumina needed to dissolve to saturate the liquid).
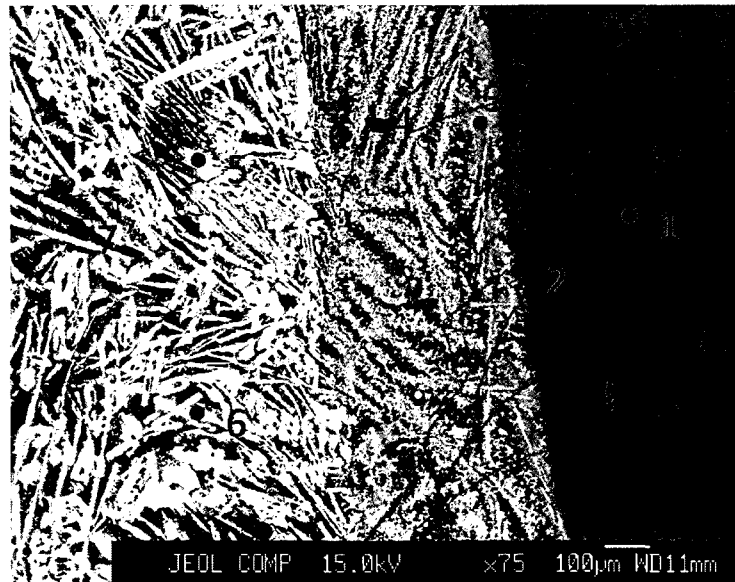
Figure 4.29 Backscattered electron image and chemical analysis points of CMS-N slag near the spindle. 1=alumina, 2=spinel, 3=Na-rich alkali calcium aluminosilicate, 4=cuspidine, 5=monticellite, 6=cuspidine, 7=Na-rich alkali calcium aluminosilicate.

The crucible region of the CMS-N slag is shown in Figure 4.30. The affected region of the crucible can again be seen as a different shade than the untouched MgO. Point 2 shows the penetration of the cuspidine phase once again into the crucible, but no difference in composition from the bulk is seen even in the slag immediately beside the crucible.
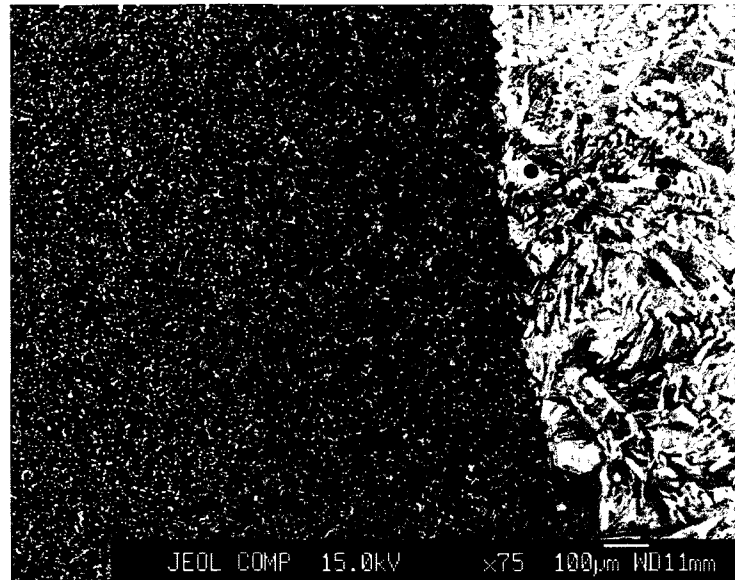
Figure 4.30 Backscattered electron image and chemical analysis points of CMS-N slag near the crucible. 1=magnesia, 2=cuspidine (containing magnesium), 3=cuspidine, 4=monticellite, 5=Na-rich alkali calcium aluminosilicate.

Figure 4.31 shows the spindle region of the CMS-K slag. The spindle in this case is surrounded by a thick layer of spinel, beyond which lies the slag. The alkali calcium aluminosilicate immediately next to the spinel barrier is depleted in Mg, since the spinel was required some MgO to form. Past this, there is little effect of the slag-spindle interaction.
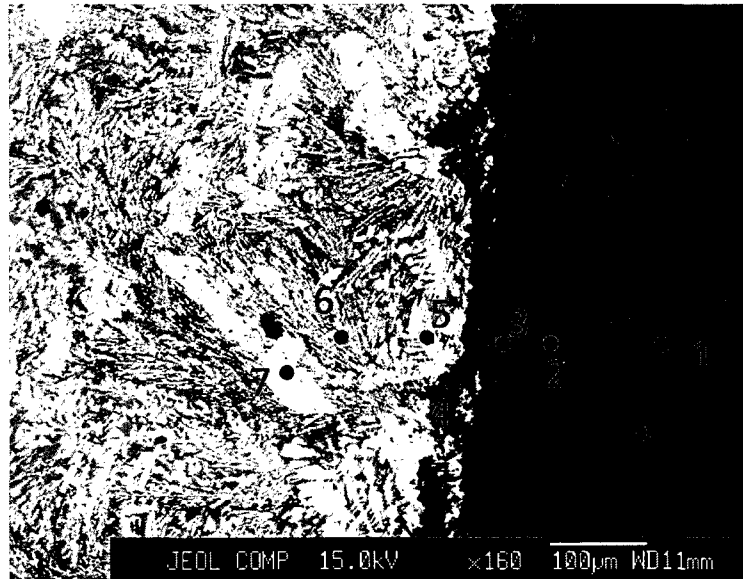
Figure 4.31 Backscattered electron image and chemical analysis points of CMS-K slag near the spindle. 1=alumina, 2=spinel, 3=spinel, 4=spinel, 5=K-rich alkali calcium aluminosilicate (containing fluorine), 6=K-rich alkali calcium aluminosilicate (containing fluorine), 7=merwinite.

The interface between the crucible and CMS-K slag is shown in Figure 4.32. The crucible is not penetrated or otherwise affected by the slag, while the slag surrounding the crucible is not enriched in Mg. There is nearly no corrosive effect of this slag on the crucible. This lessening of refractory corrosion has been observed previously with potassium-containing slags[28].
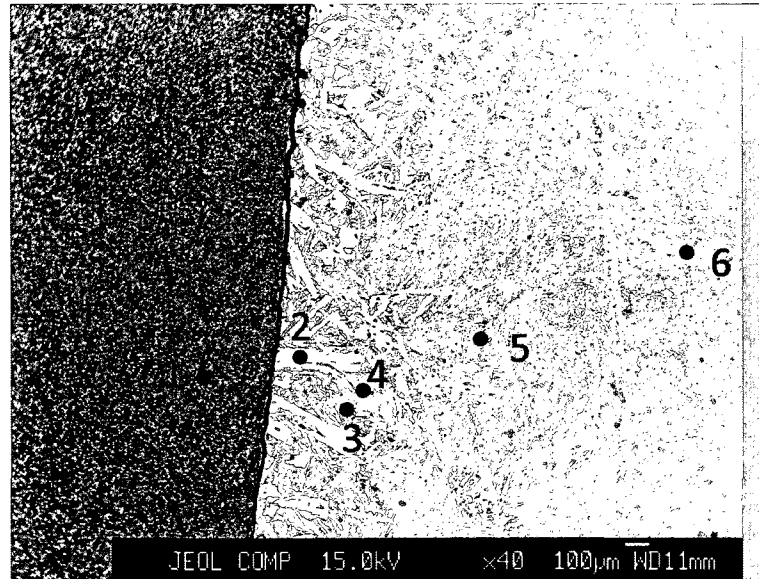
Figure 4.32 Backscattered electron image and chemical analysis points of CMS-K slag near the crucible. 1=magnesia, 2=cuspidine, 3=K-rich alkali calcium aluminosilicate (containing fluorine), 4=merwinite, 5=K-rich alkali calcium aluminosilicate (containing fluorine), 6=merwinite.

Figure 4.33 shows the spindle and CMS-HC slag near the top of the crucible. The porosity seen in the bulk slag is still evident, making identification of a large number of phases difficult. There is a layer of gehlenite apparent immediately next to the spindle, while farther away melilite occurs because of the relative depletion of Al farther from the spindle. Without the capability of testing more points in this region, the effects of the slag on the spindle are difficult to conclude.
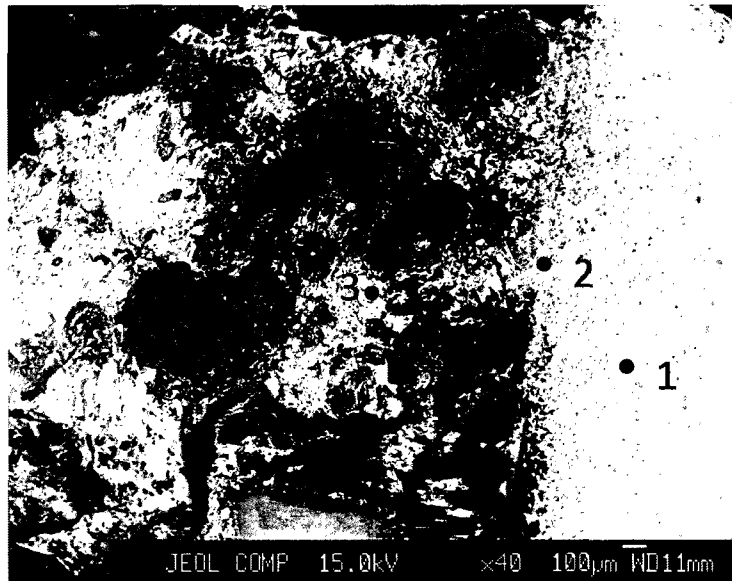
Figure 4.33 Backscattered electron image and chemical analysis points of CMS-HC slag near the spindle. 1=alumina, 2=gehlenite, 3=melilite.

Figure 4.34 shows the crucible/slag interface of the CMS-HC slag. Very little penetration of the refractory occurred, as the magnesia immediately next to the slag appears unaffected. The melilite phase closest to the crucible was slightly depleted in alumina and enriched in magnesia as compared to the bulk melilite, and the monticellite phase near the crucible contained more magnesia than the monticellite in the bulk, but the merwinite in the vicinity of the crucible was not significantly changed.
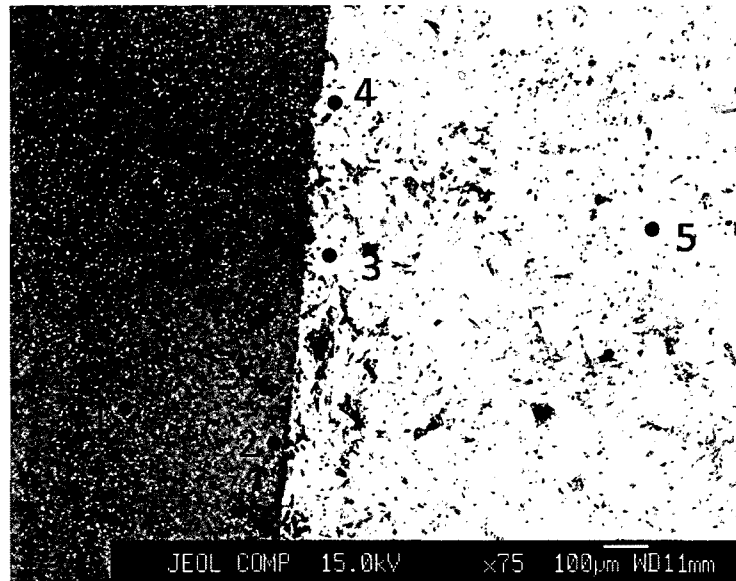
Figure 4.34 Backscattered electron image and chemical analysis points of CMS-HC slag near the crucible. 1=magnesia, 2=magnesia, 3=melilite, 4=monticellite, 5=merwinite.

4.5 SUMMARY OF RESULTS

4.5.1 CMS-F SLAG

The viscosity of the CMS-F slag was well-matched to previous tests using the same slag, and the beginning of the transition from low to high viscosity occurs at 1310 °C and 50 cP. The low viscosity of this slag at high temperature can be attributed to the high basicity of the melt, as well as the additional network-breaking effects of CaF_2. As the temperature decreased, the first phase to precipitate (at 1310 °C) from the melt was merwinite. At this point, the viscosity increased exponentially as the solid fraction of the slag increased, so that the viscosity was very high even before the entire slag had solidified.

The weight loss from this slag was 0.6% at the highest temperature, and no measured weight loss occurred below 1300 °C. Thermodynamic calculations were in excellent agreement with the weight loss result, and also showed that slag was entirely liquid at a temperature of 1310 °C. As well, two of the phases expected based on these calculations (merwinite and cuspidine) were found in the slag by XRD and by EPMA, while akermanite (which was calculated to exist) was found by XRD and not by EPMA, which instead found monticellite. There are two possible reasons for this difference. The first is that not enough points were tested in EPMA to find akermanite, and a small amount of monticellite was present (as a result of localized inhomogeneity); the second is that dissolution of the crucible in the EPMA samples was sufficient to increase the amount of MgO present in the slag, making monticellite the favoured phase.

In terms of refractory attack, the CMS-F slag had dissolved enough of the spindle to have formed discrete spinel particles within the liquid, and infiltrated the MgO crucible to a distance of approximately 700 μm, as well as dissolving some of the crucible into the adjacent slag. These effects indicate that the CMS-F slag was qualitatively the most corrosive of the slags used. Cuspidine was the phase that penetrated the MgO crucible, and one of the phases directly attacking the spindle, meaning that the inclusion of fluorine in the slag likely had a strong influence on its reactivity towards the refractory.

The use of CaF_2 in steelmaking slags has been a well-established practice for the reasons demonstrated here: the viscometric behaviour of the slag is very suitable for

steelmaking operations, the weight loss to the gas phase is quite low, and the basicity of the slag is appreciably increased. The main technical drawback of CaF_2 as a fluidizer is the effect that it has on corrosivity toward refractory phases, which is also seen here.

4.5.2 CMS-N SLAG

The CMS-N slag showed an acidic character as compared to the other slags, and had a viscosity of 70 cP at temperatures above 1435 °C. If Al_2O_3 were to be considered acidic (which it usually is in basic melts), then the CMS-N slag had significantly more acidic components (with both SiO_2 and Al_2O_3 contributing) than the CMS-F slag. This was one possible factor in the apparently acidic nature of the slag. The other is that the amount of corrosion shown by EPMA of both MgO and Al_2O_3 was extensive, which may have increased the content of one or both of these oxides in the slag to the extent that the viscosity was affected in this way.

The weight loss (which began at 1000 °C) at 1600 °C was 3.1%, and followed a similar shape as was predicted by thermodynamic calculations. The short amount of time held at temperature may have been insufficient for equilibrium to be reached, accounting for the difference between the predicted and actual weight loss. The slag was predicted to be entirely liquid above 1340 °C, below which fluorite was to begin precipitating as a solid. XRD detected several phases: anorthite (which was not predicted to form, though the predicted phases of combeite and $NaAlO_2$ in combination would form a Na-Ca-Al-Si oxide with similar composition to anorthite), merwinite, monticellite, cuspidine (which

was also not expected), and fluorite. EPMA showed that monticellite, cuspidine, and a Na-rich calcium aluminosilicate (which would represent the anorthite-type phase) were present. Similarly to the CMS-F slag, the difference could be due to dissolution of MgO in the slag, favouring monticellite over merwinite, or it could be a result of too few points being tested to find merwinite.

The high fluorine content of the slag probably contributed to the attack on the MgO and Al_2O_3 phases, since the penetrating phase (to a depth of approximately 500 μm) in the MgO was once again cuspidine, and the Na-rich calcium aluminosilicate phase and spinel phase bordering the spindle were relatively enriched in fluorine. Because the spindle corrosion appeared to be somewhat less severe than that seen in the CMS-F slag, this slag was judged to be the second-most corrosive of the four slags tested.

The CMS-N slag would not be suitable for most steelmaking operations, not only because of the acidic-type viscosity curve with a relatively high transition point, but also because of the greatly increased amount of gas produced (compared with the CMS-F slag). In addition, the corrosivity of this slag was not greatly reduced as compared to the CMS-F slag.

4.5.3 CMS-K SLAG

The viscosity-temperature curve of the CMS-K slag had a shape characteristic of a basic slag with a transition point at 1260 °C and a viscosity at higher temperature of 180 cP.

Like the CMS-F slag, the change in viscosity is probably due to the beginning of solidification rather than a change in the liquid behaviour. The first predicted phase to solidify (at 1410 °C) was fluorite, but no fluorite was found by EPMA or XRD. Instead, cuspidine, which is a less refractory phase, was found by EPMA and can be considered to have occurred in the place of fluorite as the main fluoride-bearing phase (although every grain of the K-rich calcium aluminosilicate did contain fluorine). Since the next highest-melting phase predicted to form only solidified at 1220 °C, this solidification can be used to explain the rapid increase in viscosity.

The weight loss measurements and the weight loss calculations were in good agreement about the shape of the temperature-weight loss curve for this slag, but not about the magnitude. The predicted weight loss was nearly 10%, while the measured loss was only 4.3%, which can again be attributed to the lack of equilibrium in the relatively short time at each temperature. The slag was calculated to be in liquid form above 1410 °C. As a solid, the slag was predicted to contain the phases merwinite, monticellite, akermanite, fluorite, kaliophilite ($KAlSiO_4$), and gehlenite; of these, only merwinite was found in XRD, and merwinite, cuspidine, and a K-rich calcium aluminosilicate were found in EPMA. The lack of XRD results was due to glass formation during cooling, while the phases seen in EPMA were substituting for those predicted: cuspidine for fluorite, and the K-aluminosilicate for akermanite, gehlenite, monticellite, and kaliophilite.

The corrosion of the crucible and spindle with the CMS-K slag was very limited. In the case of the spindle, an 80 μm thick layer of spinel formed that appeared to stop further diffusion or dissolution into the slag. The slag also did not penetrate the MgO refractory to any noticeable extent, meaning that very little corrosion occurred there either. These two results meant that this slag was by far the best of the four in terms of corrosivity toward MgO and Al_2O_3. This also limited the amounts of excess MgO and Al_2O_3 being brought into the liquid, making solidification of the slag at higher temperatures less likely.

The CMS-K slag would be considered a good candidate for steelmaking based on its merits shown here. The first of these is that the viscosity curve is even more favourable (having a lower transition temperature) than that of the CMS-F slag, the corrosivity of the slag toward MgO and Al_2O_3 is almost nonexistent, and the basicity of the melt is high (*potassium being a strongly basic component*). The only drawback for this slag is the large amount of vaporization inherent in its use.

4.5.4   CMS-HC AND CMS-SY SLAGS

The viscosity of the CMS-HC slag was about 70 cP above 1500 °C, and increased rapidly in viscosity below this temperature, giving the curve a shape typical of basic slags. One of the largest differences between this slag and the others is the presence of foaming (most likely due to the rapid volatilization of NaCl and KCl at high temperature). A slag of the composition that was measured after melting the slag (in Table 4-4) would have had

a solidus temperature of 1420 °C and a liquidus temperature of 1620 °C, as calculated using FACTSage, meaning that the temperatures used could not have completely melted the liquid. The explanation of the low viscosity can then be attributed to the foaming of the slag, which was visible in the crucible when microscopy was done, since a partially liquid foam would be more easily broken by the motion of the spindle. The foaming of the slag was due to evaporation of NaCl and KCl, which also accounts for the low amounts of Na, K, and Cl measured in the melted slag. The transition of the viscosity from low to high can then be explained by the reduction in foaming once the NaCl and KCl were mostly removed to the gas phase.

The weight loss measurements of the CMS-SY slag agreed with the calculated weight losses in shape, but not in absolute value. The predicted weight loss of the slag (6.7%) was about double the measured weight loss (3.2%). This weight loss began at the lowest temperature of any of the slags, around 800 °C, and had reached nearly its final value 1100 °C. Since the liquidus temperature was calculated to be much higher (1620°C) after NaCl and KCl had been lost at lower temperatures, the amount of liquid was probably reduced significantly by the time the viscometer started. The solid phases predicted were merwinite (which was found by XRD and EPMA), akermanite and gehlenite (which were present as the melilite solid solution, found by XRD and EPMA), and spinel (which was not found in XRD or EPMA). Monticellite was observed by EPMA, although it was not expected to exist; this could be a result of MgO dissolution in the slag, converting some of the merwinite to monticellite. The expected presence of spinel would have also

been a factor in viscometry, since spinel would be solid throughout the test temperature range.

The corrosivity of the slag toward the MgO and Al_2O_3 refractories was relatively less than the CMS-F and CMS-N slags, but more than when the CMS-K slag was used. The lack of penetration into the MgO crucible was positive from the corrosion standpoint, but there was still some amount of MgO dissolved into the nearby slag. The effect that the slag had on the alumina spindle was less easy to determine, but it was clear that there was no catastrophic dissolution or penetration of the alumina, while a layer of gehlenite was formed on the alumina, indicating some reaction between slag and spindle.

Spent salt was a good fluidizer in some senses: the viscosity curve of the slag had a transition point low enough to be useful in steelmaking, and the corrosion of the refractories was less pronounced than in the CMS-F slag. On the other hand, the amount of gas produced (even at low temperatures) was relatively high, and the viscosity underwent significant changes as the volatile components of the melt were removed from the liquid. The viscosity measurements indicated a basic character to the slag as well, and even once the volatile components were removed, the slag could be expected to melt completely near the usual steelmaking temperature range (around 1620 °C), after which this basic character would be expected to be conserved.

5.0 CONCLUSIONS

After consideration of the results, several conclusions can be made about the behaviour and characteristics of the slags used. These conclusions can be sorted into three categories: conclusions regarding slag viscosity; conclusions regarding slag composition, weight loss, and mineralogy; and conclusions regarding the potential usefulness of a slag of these types in industrial practice.

Regarding slag viscosity, the CMS-K, CMS-F, and CMS-HC slags all showed behaviour typical of basic slags, while the CMS-N slag showed a more acidic shape. The CMS-K slag had the lowest temperature transition between low and high viscosity, followed by the CMS-F, CMS-N, and CMS-HC slags. The viscosity of the CMS-F and CMS-K slags were primarily determined by the precipitation of solids with decreasing temperature, the viscosity of the CMS-N slag was determined by the more acidic nature of the melt, and the viscosity of the CMS-HC slag was determined by the amount of volatile phases which had left the liquid phase.

The slag composition and mineralogy were both determined to a large extent by the non-fluidizing components. Because of this, all of the slags were found to contain CaO-SiO_2 rich phases (such as merwinite, cuspidine, monticellite, or melilite). The fluidizing components contributed greatly to the weight loss of the slags, with the changes in chemistry of the slags occurring primarily by the loss of sodium and potassium halides upon heating. The difference between fluoride and chloride additions also had a

profound effect, with the fluorides additions causing a lower transition temperature, and the chloride addition causing much more volatility at lower temperatures.

In terms of usefulness to industry, the CMS-K and CMS-HC slags showed promise: the viscosity of each slag was low in an appropriate range of temperatures for steelmaking, and neither slag was found to be very corrosive to refractory materials. Both of these slags did have significant weight losses at high temperatures, however. The CMS-N slag did not perform as well in viscosity or corrosion evaluation, and was about equivalent to the CMS-K slag in weight loss, meaning that it was not an ideal candidate for steelmaking slag use.

6.0 REFERENCES

1. World Steel Association. Online at: www.worldsteel.org. Accessed on: February 24 2010.

2. R.J. Fruehan (1985). Ladle Metallurgy Principles and Practice. Iron and Steel Society of A.I.M.E.

3. W.T. Lankford Jr., N.L. Samways, R.F. Craven, H.E. McGannon, eds. (1985). The Making, Shaping and Treating of Steel. 10th edition, United States Steel, Pittsburgh, Pennsylvania.

4. T. Rosenqvist (2004). Principles of Extractive Metallurgy. 2nd edition, Tapir Academic Press, Trondheim, Norway.

5. International Aluminium Institute. Online at: www.world-aluminium.org. Accessed on: March 8, 2010.

6. K. Grjotheim, C. Krohn, M. Malinovsky, K. Matiasovsky, J. Thonstad (1977). Aluminum Electrolysis: The Chemistry of the Hall-Héroult Process. Aluminium-Verlag GmbH, Dusseldorf.

7. W.J. Bruckard, J.T. Woodcock (2007). *Characterisation and treatment of Australian salt cakes by aqueous leaching*. Minerals Engineering. Vol. 20, pp. 1376-1390.

8. M.J. Magyar, R.S. Kaplan, H.V. Makar (1980). *Experimental processing of salt slags from an aluminum dross furnace*. Report of Investigations – United States, Bureau of Mines, No. 8446.

9. J.N. Hryn, G.K. Krumdick (2002). *Recycling aluminum salt cake*. Light Metals: Proceedings of Sessions, TMS Annual Meeting, pp. 1053.

10. D.F. Lisbona, K.M. Steel (2008). *Recovery of fluoride values from spent pot-lining: Precipitation of an aluminium hydroxyfluoride hydrate product*. Separation and Purification Technology Vol. 61, pp. 182–192.

11. D. Miksa, M. Homsak, N. Samec (2003). *Spent potlining utilisation possibilities*. Waste Management & Research, Vol. 21, pp. 467-473.

12. V. Spironello (1982). *Evaluation of used aluminum smelter potlining as a substitute for fluorspar in basic oxygen steelmaking*. Report of Investigations – United States Bureau of Mines, No. 8699.

13. V. Spironello (1983). *Evaluation of aluminum smelter potlining as a substitute for fluorspar in cupola ironmelting and basic oxygen steelmaking*. Report of Investigations – United States Bureau of Mines, No. 8775

14. D. Augood (1989). *Use of spent potlining as flux in making steel.* Light Metals: Proceedings of Sessions, TMS Annual Meeting, pp. 395-398.

15. H. Hu, R.G. Reddy (1989).*Viscosity of molten spent potlining.* Light Metals: Proceedings of Sessions, TMS Annual Meeting, pp. 801-803.

16. J.H. Park, H. Kim, D.J. Min (2008). *Novel Approach to Link between Viscosity and Structure of Silicate Melts via Darken's Excess Stability Function: Focus on the Amphoteric Behavior of Alumina.* Metallurgical and Materials Transactions B, Vol. 39B, pp. 150-153.

17. D. R. Poirier, G. H. Geiger (1994). Transport phenomena in materials processing. Minerals, Metals & Materials Society.

18. K.C. Mills (1992). *The Influence of Structure on the Physico-chemical properties of slags.* ISIJ International, Vol. 3, No. 1, pp.148-155.

19. J.H. Park, D.J. Min (2004). *Effect of fluorspar and alumina on the viscous flow of calcium silicate melts containing MgO.* Journal of Non-Crystalline Solids Vol. 337, pp. 150–156.

20. C.W. Bale, P. Chartrand, S.A. Degterov, G. Eriksson, K. Hack, R. Ben Mahfoud, J. Melançon, A.D. Pelton, S. Petersen. *FactSage Thermochemical Software and Databases.* Calphad, Vol. 26, No. 2, pp. 189-228, 2002.

21. E.M. Levin, C.R. Robbins, H.F. McMurdie (1964). Phase Diagrams for Ceramists. The American Ceramic Society, Columbus, Ohio.

22. J.R. MacLean, P.W. Kingston, J.B. MacDonald, W.F. Caley (1997). *Potential role of feldspar/feldspathoid minerals in secondary steelmaking.* Ironmaking and Steelmaking. Vol. 24, No. 5, pp. 406-411.

23. T.S. Tribe, P.W. Kingston, J.B. MacDonald, W.F. Caley (1994). *Reduction of Fluorspar Consumption in Secondary Steelmaking.* Ironmaking and Steelmaking. Vol. 21, No. 2, pp. 145–149.

24. W.F. Caley, D. Weisgerber, G.J. Kipouros, S.W. Robinson (2004). *Mineral additives as slag modifiers.* AISTech Proceedings, Vol. 1, pp. 783-795.

25. J.R. Van Wazer, J.W. Lyons, K.Y. Kim, R.E. Colwell (1963). Viscosity and Flow Measurement: A Laboratory Handbook of Rheology. John Wiley and Sons, Inc., New York, New York.

26. Brookfield Engineering Laboratories Inc. (1985) *More Solutions to Sticky Problem: A guide to getting more from your Brookfield viscometer.* Brookfield Engineering Inc., Stoughton, Massachusetts.

27. W. F. Caley, J. B. MacDonald, G. J. Kipouros. *Rheological, Mineralogical and Fluxing Aspects of Steelmaking Slags.* The International George N. Papatheodorou Symposium. Ed. S. Boghosian, V. Dracopoulos, C.G. Kontoyannis, G.A. Voyiatzis. pp. 120-124, Patras, Greece, September 17-18, 1999.

28. J.R. MacLean (1995). The use of feldspar/feldspathoid minerals as a fluorspar replacement in secondary steelmaking. M.A.Sc. thesis, Technical University of Nova Scotia.

29. Y. Sasaki, M. Iguchi, M. Hino (2007). *The Role of Ca and Na Ions in the Effect of F Ion on Silicate Polymerization in Molten Silicate System.* ISIJ International, Vol. 47, No. 5, pp. 638–642.

30. S. Wright, L. Zhang, S. Sun, S. Jahanshahi (2000). *Viscosity of a CaO-MgO-Al2O3-SiO2 Melt Containing Spinel Particles at 1646 K.* Metallurgical and Materials Transactions B, Vol. 31B, pp. 97-104.

31. A.L. Leal-Cruz, M.I. Pech-Canul, M.T. Certucha-Barragan (2008). *A different consideration for Na2SiF6 formation/dissociation and its relation with silicon fluoride vaporization in the steelmaking process.* Mineral Processing and Extractive Metallurgy Review, Vol. 29, No. 4, pp. 318-329.

32. M. Persson, S. Seetharaman, S. Seetharaman (2007). *Kinetic studies of fluoride evaporation from slags.* ISIJ International, Vol. 47, No. 12, pp. 1711–1717.

APPENDIX A: EPMA CHEMICAL ANALYSIS

EPMA point scan chemistry is shown in Table A-1 and

Table A-2, by weight percent and atomic percent, respectively.

Table A-1 Quantitative chemical compositions, by weight percent, for point scans done with EPMA. Note that B indicates an image of the bulk, B(b) an image taken near the bottom of the crucible, B(t) an image near the top of the crucible, M an image near the metallic phase in the CMS-HC slag, C an image showing the crucible/slag interface, and S an image showing the spindle/slag interface.

Slag	Image	Point	K	Cl	Mg	Al	Ca	Na	Si	F	O	Total
CMS-F	B	1	0.0	0.0	0.6	0.0	43.1	0.0	14.5	0.5	34.9	93.8
CMS-F	B	2	0.0	0.0	7.7	0.0	37.2	0.0	16.6	0.0	40.2	101.7
CMS-F	B	3	0.0	0.0	16.5	0.1	25.3	0.0	17.4	0.0	42.4	101.6
CMS-F	C	1	0.0	0.0	63.8	0.0	0.1	0.0	0.0	0.0	43.3	107.2
CMS-F	C	2	0.0	0.0	2.5	0.0	38.6	0.0	12.7	0.1	35.6	89.5
CMS-F	C	3	0.0	0.0	63.6	0.0	0.1	0.0	0.0	0.0	43.0	106.6
CMS-F	C	4	0.0	0.0	11.0	0.1	34.7	0.0	12.7	0.3	35.6	94.3
CMS-F	S	1	0.0	0.0	0.0	53.1	0.0	0.0	0.0	0.0	50.0	103.2
CMS-F	S	2	0.0	0.0	0.9	0.1	42.9	0.0	14.6	0.5	35.9	94.9
CMS-F	S	3	0.0	0.0	0.6	18.1	29.5	0.0	10.6	0.0	43.1	101.9
CMS-F	S	4	0.0	0.0	18.3	37.8	0.1	0.0	0.0	0.0	47.1	103.1
CMS-F	S	5	0.0	0.0	16.7	0.1	24.9	0.0	17.2	0.0	41.6	100.5
CMS-F	S	6	0.0	0.0	0.7	0.0	43.5	0.0	14.5	0.4	35.1	94.2
CMS-K	S	1	0.0	0.0	0.0	53.3	0.0	0.0	0.0	0.0	49.9	103.2
CMS-K	S	2	0.5	0.0	13.8	27.7	9.9	0.0	3.7	0.1	46.7	102.4
CMS-K	S	3	0.6	0.0	15.6	30.3	7.3	0.0	3.2	0.1	45.6	102.7
CMS-K	S	4	0.7	0.0	18.5	36.6	0.6	0.0	0.2	0.0	49.5	106.0
CMS-K	S	5	2.0	0.0	1.2	0.8	41.4	0.0	11.0	0.8	25.0	82.1
CMS-K	S	6	6.0	0.0	8.9	5.2	24.8	0.0	12.6	0.4	36.4	94.4
CMS-K	S	7	0.1	0.0	7.7	0.0	37.0	0.0	16.1	0.0	40.3	101.3
CMS-K	B	1	0.1	0.0	7.8	0.0	36.9	0.0	16.7	0.0	40.5	102.0
CMS-K	B	2	0.2	0.0	1.0	0.2	43.0	0.0	14.6	0.6	35.4	94.9
CMS-K	B	3	6.4	0.0	8.4	6.0	24.2	0.0	12.9	0.5	35.3	93.9
CMS-K	C	1	0.0	0.0	63.6	0.0	0.1	0.0	0.0	0.0	42.9	106.6
CMS-K	C	2	0.1	0.0	0.7	0.0	43.4	0.0	14.5	0.6	35.4	94.8
CMS-K	C	3	4.9	0.0	6.2	4.4	29.1	0.0	13.5	0.4	37.1	95.7
CMS-K	C	4	0.2	0.0	7.8	0.0	36.9	0.0	16.4	0.0	40.5	101.8
CMS-K	C	5	6.4	0.0	10.6	6.1	21.7	0.0	12.1	0.4	36.8	94.0
CMS-K	C	6	0.1	0.0	7.7	0.0	36.9	0.0	16.5	0.0	40.1	101.3
CMS-HC	S	1	0.0	0.0	0.0	52.2	0.0	0.0	0.1	0.0	50.0	102.3
CMS-HC	S	2	0.0	0.1	0.6	17.2	28.5	0.2	10.3	0.0	38.1	95.0
CMS-HC	S	3	0.0	0.1	4.9	8.5	29.1	0.1	14.8	0.0	40.7	98.2
CMS-HC	B(b)	1	0.0	0.1	7.8	0.0	38.0	0.1	16.6	0.0	40.6	103.1

CMS-HC	B(b)	2	0.0	0.2	16.4	0.0	26.0	0.1	17.2	0.0	41.1	101.1
CMS-HC	B(b)	3	0.0	0.1	4.1	10.5	30.3	0.1	14.5	0.0	42.4	101.9
CMS-HC	B(b)	4	0.9	4.1	2.8	11.0	29.6	0.1	12.6	0.0	27.7	88.7
CMS-HC	M	1	0.1	0.1	0.0	11.8	0.1	0.0	3.2	0.2	1.1	16.6
CMS-HC	M	2	0.0	0.2	3.9	9.6	28.5	0.1	16.4	0.0	40.4	99.1
CMS-HC	M	3	0.0	0.0	16.6	0.0	25.6	0.0	17.4	0.0	41.7	101.4
CMS-HC	C	1	0.0	0.1	62.0	0.0	0.2	0.0	0.1	0.0	40.6	102.9
CMS-HC	C	2	0.0	0.0	62.6	0.0	0.1	0.0	0.0	0.0	41.5	104.2
CMS-HC	C	3	0.0	0.1	6.0	5.1	33.4	0.1	16.2	0.0	41.8	102.8
CMS-HC	C	4	0.0	0.0	17.1	0.1	24.8	0.0	17.7	0.0	42.3	102.0
CMS-HC	C	5	0.0	0.1	7.9	0.0	37.4	0.1	16.8	0.0	40.1	102.3
CMS-HC	B(t)	1	0.0	0.1	5.0	8.6	29.5	0.1	15.8	0.0	41.6	100.7
CMS-HC	B(t)	2	0.0	0.0	17.2	0.1	24.5	0.0	17.5	0.0	41.1	100.4
CMS-N	S	1	0.0	0.0	0.0	52.8	0.0	0.0	0.0	0.0	48.7	101.5
CMS-N	S	2	0.0	0.0	18.9	25.6	0.6	5.3	4.2	0.4	47.0	102.0
CMS-N	S	3	0.0	0.0	1.3	11.3	19.4	7.4	15.2	0.3	49.6	104.6
CMS-N	S	4	0.0	0.0	0.8	0.3	42.7	0.2	14.3	0.6	33.8	92.8
CMS-N	S	5	0.0	0.0	16.2	0.0	26.1	0.0	17.2	0.0	41.7	101.3
CMS-N	S	6	0.0	0.0	0.5	0.2	43.8	0.1	14.4	0.5	35.0	94.5
CMS-N	S	7	0.1	0.0	12.9	12.3	2.1	3.6	9.0	0.5	33.2	73.6
CMS-N	B	1	0.0	0.0	0.5	0.1	43.7	0.1	14.6	0.6	35.1	94.7
CMS-N	B	2	0.0	0.0	16.3	0.0	26.0	0.0	17.6	0.0	41.9	101.8
CMS-N	B	3	0.0	0.0	61.5	0.0	0.1	0.1	0.0	0.0	41.8	103.6
CMS-N	C	1	0.0	0.0	63.3	0.0	0.1	0.1	0.0	0.0	42.4	105.8
CMS-N	C	2	0.0	0.0	6.4	0.1	19.6	0.6	8.4	0.0	28.0	63.2
CMS-	C	3	0.0	0.0	0.5	0.0	43.5	0.1	14.4	0.5	35.2	94.3

N											
CMS-N	C	4	0.0	0.0	16.2	0.0	26.0	0.1	17.4	0.0	43.0	102.7
CMS-N	C	5	0.0	0.0	14.6	13.7	2.3	3.0	9.1	0.5	48.2	91.4

Table A-2 Quantitative chemical compositions, by atomic percent, for point scans done with EPMA. Note that B indicates an image of the bulk, B(b) an image taken near the bottom of the crucible, B(t) an image near the top of the crucible, C an image showing the crucible/slag interface, and S an image showing the spindle/slag interface.

Slag	Image	Point	K	Cl	Mg	Al	Ca	Na	Si	F	O	Total
CMS-F	B	1	0.0	0.0	0.7	0.0	28.1	0.0	13.5	0.7	57.0	100.0
CMS-F	B	2	0.0	0.0	7.3	0.0	21.3	0.0	13.6	0.0	57.8	100.0
CMS-F	B	3	0.0	0.0	14.8	0.1	13.8	0.0	13.5	0.0	57.8	100.0
CMS-F	C	1	0.0	0.0	49.2	0.0	0.0	0.0	0.0	0.0	50.7	100.0
CMS-F	C	2	0.0	0.0	2.7	0.0	25.7	0.0	12.1	0.1	59.4	100.0
CMS-F	C	3	0.0	0.0	49.3	0.0	0.0	0.0	0.0	0.0	50.7	100.0
CMS-F	C	4	0.0	0.0	11.3	0.1	21.6	0.0	11.2	0.4	55.4	100.0
CMS-F	S	1	0.0	0.0	0.0	38.7	0.0	0.0	0.0	0.0	61.3	100.0
CMS-F	S	2	0.0	0.0	0.9	0.1	27.5	0.0	13.3	0.7	57.5	100.0
CMS-F	S	3	0.0	0.0	0.6	14.9	16.3	0.0	8.4	0.0	59.8	100.0
CMS-F	S	4	0.0	0.0	14.7	27.5	0.0	0.0	0.0	0.0	57.8	100.0
CMS-F	S	5	0.0	0.0	15.2	0.1	13.7	0.0	13.5	0.0	57.5	100.0
CMS-F	S	6	0.0	0.0	0.7	0.0	28.2	0.0	13.4	0.6	57.0	100.0
CMS-K	S	1	0.0	0.0	0.0	38.8	0.0	0.0	0.0	0.0	61.2	100.0
CMS-K	S	2	0.3	0.0	11.6	20.9	5.0	0.0	2.7	0.1	59.4	100.0
CMS-K	S	3	0.3	0.0	13.0	22.8	3.7	0.0	2.3	0.1	57.8	100.0
CMS-K	S	4	0.3	0.0	14.5	25.9	0.3	0.0	0.1	0.0	58.9	100.0
CMS-K	S	5	1.6	0.0	1.6	0.9	32.7	0.0	12.4	1.4	49.5	100.0
CMS-K	S	6	3.8	0.0	8.9	4.7	15.2	0.1	11.0	0.5	55.8	100.0
CMS-K	S	7	0.1	0.0	7.3	0.0	21.3	0.0	13.2	0.0	58.1	100.0
CMS-K	B	1	0.1	0.0	7.3	0.0	21.1	0.0	13.6	0.0	57.9	100.0
CMS-K	B	2	0.2	0.0	1.0	0.2	27.6	0.0	13.3	0.8	56.9	100.0
CMS-K	B	3	4.1	0.0	8.6	5.5	15.0	0.1	11.4	0.6	54.7	100.0
CMS-K	C	1	0.0	0.0	49.3	0.0	0.0	0.0	0.0	0.0	50.6	100.0
CMS-K	C	2	0.1	0.0	0.7	0.0	27.9	0.0	13.3	0.8	57.1	100.0
CMS-K	C	3	3.1	0.0	6.2	3.9	17.8	0.0	11.7	0.6	56.7	100.0
CMS-K	C	4	0.1	0.0	7.3	0.0	21.1	0.0	13.4	0.0	58.0	100.0
CMS-K	C	5	4.0	0.0	10.6	5.4	13.1	0.1	10.5	0.5	55.8	100.0
CMS-K	C	6	0.1	0.0	7.3	0.0	21.2	0.0	13.5	0.0	57.9	100.0
CMS-HC	S	1	0.0	0.0	0.0	38.2	0.0	0.0	0.0	0.0	61.7	100.0
CMS-HC	S	2	0.0	0.1	0.6	15.4	17.2	0.2	8.9	0.0	57.6	100.0
CMS-HC	S	3	0.0	0.1	4.6	7.3	16.8	0.1	12.2	0.0	58.9	100.0
CMS-HC	B(b)	1	0.0	0.0	7.3	0.0	21.5	0.1	13.4	0.0	57.6	100.0
CMS-HC	B(b)	2	0.0	0.1	14.9	0.0	14.3	0.1	13.6	0.0	56.9	100.0
CMS-HC	B(b)	3	0.0	0.1	3.7	8.6	16.8	0.1	11.5	0.0	59.1	100.0
CMS-HC	B(b)	4	0.6	3.2	3.2	11.4	20.6	0.1	12.5	0.0	48.4	100.0

CMS-HC	M	1	0.4	0.2	0.1	68.3	0.5	0.2	17.6	1.8	11.0	100.0
CMS-HC	M	2	0.0	0.1	3.7	8.2	16.4	0.1	13.5	0.0	58.1	100.0
CMS-HC	M	3	0.0	0.0	15.0	0.0	14.0	0.0	13.6	0.0	57.3	100.0
CMS-HC	C	1	0.0	0.0	50.0	0.0	0.1	0.0	0.0	0.0	49.8	100.0
CMS-HC	C	2	0.0	0.0	49.8	0.0	0.1	0.0	0.0	0.0	50.1	100.0
CMS-HC	C	3	0.0	0.1	5.6	4.2	18.6	0.1	12.9	0.0	58.5	100.0
CMS-HC	C	4	0.0	0.0	15.3	0.1	13.5	0.0	13.7	0.0	57.4	100.0
CMS-HC	C	5	0.0	0.0	7.4	0.0	21.4	0.1	13.7	0.0	57.4	100.0
CMS-HC	B(t)	1	0.0	0.0	4.6	7.2	16.6	0.1	12.7	0.0	58.7	100.0
CMS-HC	B(t)	2	0.0	0.0	15.6	0.1	13.5	0.0	13.8	0.0	56.9	100.0
CMS-N	S	1	0.0	0.0	0.0	39.1	0.0	0.0	0.0	0.0	60.8	100.0
CMS-N	S	2	0.0	0.0	15.3	18.7	0.3	4.5	2.9	0.4	57.9	100.0
CMS-N	S	3	0.0	0.0	1.1	8.5	9.8	6.5	11.0	0.3	62.8	100.0
CMS-N	S	4	0.0	0.0	0.9	0.3	28.2	0.3	13.5	0.8	56.0	100.0
CMS-N	S	5	0.0	0.0	14.7	0.0	14.3	0.0	13.5	0.0	57.4	100.0
CMS-N	S	6	0.0	0.0	0.5	0.2	28.4	0.1	13.3	0.7	56.8	100.0
CMS-N	S	7	0.1	0.0	14.7	12.6	1.4	4.4	8.8	0.7	57.3	100.0
CMS-N	B	1	0.0	0.0	0.5	0.1	28.2	0.1	13.4	0.8	56.8	100.0
CMS-N	B	2	0.0	0.0	14.7	0.0	14.2	0.0	13.7	0.0	57.3	100.0
CMS-N	B	3	0.0	0.0	49.1	0.0	0.0	0.1	0.0	0.0	50.8	100.0
CMS-N	C	1	0.0	0.0	49.5	0.0	0.0	0.1	0.0	0.0	50.4	100.0
CMS-N	C	2	0.0	0.0	9.3	0.2	17.3	0.9	10.6	0.1	61.7	100.0
CMS-N	C	3	0.0	0.0	0.6	0.0	28.2	0.1	13.3	0.7	57.1	100.0
CMS-N	C	4	0.0	0.0	14.4	0.0	14.1	0.1	13.4	0.0	58.1	100.0
CMS-N	C	5	0.0	0.0	12.8	10.9	1.3	2.8	7.0	0.6	64.6	100.0

APPENDIX B: VISCOSITY MEASUREMENT DATA

The raw data from slag viscosity testing is shown in the electronic appendices.

APPENDIX C : FACTSAGE THERMODYNAMIC CALCULATIONS

The raw data from thermodynamic calculations using FACTSage are shown in the electronic appendices.